EARTHQUAKE RESPONSE OF R/C FRAMES WITH REINFORCED INFILL WALLS

A Thesis Submitted to the
Graduate School of Engineering and Sciences of
İzmir Institute of Technology
in Partial Fulfillment of the Requirements for the Degree of

MASTER OF SCIENCE

in Civil Engineering
Structural Mechanics

by
Umut YILDIRIM

July 2008
İZMİR

We approve the thesis of **Umut YILDIRIM**

Assist. Prof. Dr. Gürsoy TURAN
Supervisor

Assist. Prof. Dr. Özgür Oğuz EĞİLMEZ
Committee Member

Assist. Prof. Dr. Ayhan NUHOĞLU
Committee Member

15 July 2008

Prof. Dr. Gökmen TAYFUR
Head of Department of Civil Engineering
İzmir Institute of Technology

Prof. Dr. Hasan BÖKE
Dean of the Graduate School of
Engineering and Sciences

ACKNOWLEDGEMENTS

I would like to express my great admiration and send my special thanks to my supervisor Asst. Prof. Dr. Gürsoy TURAN for his precious patience, guidance and effort of teaching desire throughout my thesis and graduation. This thesis would not be completed without his support.

I also would like to thank to other members of the thesis committee Asst. Prof. Dr. Özgür Oğuz EĞİLMEZ and Asst. Prof. Dr. Ayhan NUHOĞLU.

I also would like to thank to my tutors Asst. Prof. Dr. Cemalettin DÖNMEZ, Asst. Prof. Dr. Engin AKTAŞ, Prof. Dr. Gökmen TAYFUR, Asst. Prof. Dr. İsfendiyar EGELİ, Asst. Prof. Dr. Özgür Oğuz EĞİLMEZ of sharing their knowledge and providing me a new point of view to my life and profession.

I also would like to thank to Asst. Prof. Dr. Selçuk SAATÇİ for his guidance with Vector2.

I also would like to thank to Uyum Yapı Denetim Ltd. Sti., for their permission to study my lectures. I thank to my colleagues for their extra hard-working instead of me, especially to Serkan GÜLECEN and Fazıl Murat EŞREFOĞLU.

I also would like to thank to Umutlab Laboratory for their support in testing facilities.

I also would like to thank to Gökçe KINAY for her support.

Finally, I send my special thanks to my family, for all their love and wonderful support for their big boy.

ABSTRACT

EARTHQUAKE RESPONSE OF R/C FRAMES WITH REINFORCED INFILL WALLS

Most of the reinforced concrete structures that are built in the past few decades are in lack of ductility and lateral stiffness. In the content of the present work, a fast and economical remedy was searched to rehabilitate these type of buildings that are under high risk of earthquake damage.

The strengthening technique needs to be finished in a short time without the people that live inside the buildings to move out. Furthermore, the chosen strengthening technique needs to be economical enough so that the home owner would not hesitate in making a decision of the rehabilitation.

In regard of the above mentioned two criteria, existing infill clay brick walls may be strengthened by the addition of a wire mesh on the surface together with a layer of plaster. In order to investigate its effectiveness, a numerical investigation is carried out to study the behaviour of a strengthened infilled reinforced concrete (RC) frame using wire mesh under lateral reversed cyclic loading. A single span, one-story clay brick infilled RC frame is modeled and a nonlinear analysis is made.

The analysis results indicate that the technique of strengthening with wire mesh increased the peak lateral load, ductility and energy dissipation.

ÖZET

GÜÇLENDİRİLMİŞ OLAN DOLGU DUVARLARA SAHİP BETONARME ÇERÇEVELERİN DEPREM DAVRANIŞI

Geçen birkaç on yıllık sürede inşa edilen betonarme binaların çoğu süneklilik ve yanal rijitlik açısından yeterli değildir. Mevcut çalışma kapsamında, bu tip binaların depremden zarar görme riskleri yüksek olduğu için, hızlı ve ekonomik bir çözüm araştırıldı.

Güçlendirme tekniğinin seçiminde binada yaşayan insanların taşınmasına gerek kalmadan kısa sürede bitirilmesine önem verilmelidir. Ayrıca seçilen güçlendirme tekniği yeteri kadar ekonomik olup, mal sahibinin vakit kaybetmeden onarımı yaptırması sağlanmalıdır.

Yukarıda bahsedilen iki kıstasların ışığında tel ızgaralarla güçlendirilmiş dolgu betonarme çerçevelerin yanal tersinir döngüsel yükleme altındaki davranışını incelemek için nümerik analiz uygulanmıştır. Bahsi geçen çalışmada tek açıklıklı, tek katlı kil tuğla ile doldurulmuş betonarme çerçeve modellendi ve doğrusal olmayan analiz yapıldı.

Analiz sonuçları tel ızgaralarla güçlendirme tekniğinin yanal yükün en büyük değerini, sünekliği ve enerji sönümlemesinin arttığını göstermiştir.

TABLE OF CONTENTS

LIST OF FIGURES

Figure **Page**

LIST OF TABLES

Table **Page**

CHAPTER 1

INTRODUCTION

1.1. Overview

A great majority of reinforced concrete (RC) structures in Turkey were severely damaged or collapsed during ground motions. Thousands of people died after recent earthquakes. The main reasons of these losses originate from the fact that the average of the structures in Turkey are not well engineered and also some of them are constructed illegally. Besides the mentioned cases, existing structures still have similar deficiencies for future hazardous earthquake loads. Reliable strengthening methodologies and rehabilitation procedures should be established as quickly as possible to minimize the expected loss in the future.

Different strengthening methods (addition of shear walls, precast panels, steel bracing, concrete jacketing of frames, etc.) have been used. Among these techniques, addition of RC shear (infill) walls was found practical and economical in Turkey. RC infilled frame increases the lateral load capacity of the RC frame and reduces the lateral displacement (drift) at ultimate load. However, the construction work for these applications lengthen the retrofit time and occupants of the rehabilitated buildings have to be relocated. Reconstruction may disturb the ongoing building facilities and new structural elements may affect the architectural aesthetics of the structures. These restorations may add considerable mass and cause high seismic (lateral) loads during an earthquake. And also, altering the dimension of the RC frame leads to take more loads of the RC frame members. In order to overcome these deficiencies, new alternative retrofit strategies are needed.

Infill walls are commonly used in low and mid-rise constructions in Turkey. They are generally used as interior partitions or exterior walls in buildings. Partition walls are usually treated as non-structural elements and often ignored in design. Recent studies have shown that infilled RC frames can be superior to a bare RC frame in terms of stiffness, ductility and energy dissipation (Shing, et al. 2002).

By recent improvements in polymer composite technology; the infill walls can be strengthened and retrofitted with fiber reinforced polymers (FRP). FRP brings logical solutions because of their small thickness, ease of application and advantage of high strength. Moreover, the strength and stiffness of a structure can be increased with little mass. Nevertheless, use of fiber reinforced polymers is limited due to economic factors, lack of standards and some doubts of serviceability life. (Canbay, et al. 2003, Türk, et al. 2003, Saatcıoglu 2006, Anıl, et al. 2006, Binici, et al. 2007, Altın, et al. 2007).

As a matter of fact, it is known that most of the people live in inadequate economic conditions. Thus, the usage of fiber reinforced polymers (FRP), as being a reliable strengthening method, may not be an option to most of the home owners, simply because of its high cost. Assessment of strengthening the large number of infill walls could be economical and would be superior to other techniques.

An investigation was carried out on previous similar studies of cyclically loaded reinforced concrete frame of which infill walls are reinforced by mortar or concrete jacketing. In this study, the performance of wall and columns that are rehabilitated by jacketing was observed. In this system, walls are confined through vertical and horizontal RC tie-columns and bond-beams. If confinement location and detailing are standard this system has performed excellently under very intense earthquakes. But severe damage was observed when confinement detailing were substandard. For such cases, wall jacketing is one rehabilitation technique suitable for improving its lateral strength and stiffness. Jacketed specimens showed uniform distribution of cracks and increased strength was seen compared to the bare frames. To achieve any benefit from wall jacketing, careful and detailed installation of fasteners should be applied. Steel nails were used to fasten the steel wire mesh. Fasteners were placed at the grid intersections of the wire mesh. They were placed by hammering them into the wall. The nail head was bent at the wire intersection to secure the mesh in position. Spacers or metal washers used between the wall and the mesh according to fastening technique (Alcocer 1996).

1.2. Assessment of The Analysis

If the buildings that were built several years ago were to be evaluated by today's design code, unfortunately, many of them would be considered inadequate in strength and ductility. There are generally two common deficiencies which is related to shear and moment capacity of these buildings. In contrast to moment failure, shear critical buildings are associated with a brittle failure mechanism and it is apparent that the shear failure could be more significant than the moment failure. Some theoretical models are developed such as Compression Field and Modified Compression Field theories to understand the shear behaviour principle.

In the past decades, most of the RC structures were often designed on the assumption of linear-elastic principles. The lack of ductility in the buildings mainly arises due to incorrect joint connections and/or insufficient confinement.

Therefore a more comprehensive structural analysis (nonlinear) is required to reassess the capacity of rehabilitated structures according to current standards. For rehabilitated buildings, second order effects have to be taken into account such as material and geometric nonlinearities. These effects could influence the ultimate capacity and failure mode. Therefore, elastic analysis may not be useful for a rehabilitation strategy.

The software utilized in the current analysis is Vector2, a nonlinear finite element program which is developed at the University of Toronto and is based on the Modified Compression Field Theory (MCFT) (Wong and Vecchio 2002).

1.3. Finite Element Program

The infill wall was modelled and simulated by a nonlinear analysis program, Vector2. Analytical results were compared to changes in lateral load capacity and stiffness of the RC frame models. Vector2 is a nonlinear finite element program that is capable of analyzing two dimensional structures subjected to quasi-static loads. This program utilizes rotational crack formulation for reinforced concrete which is based on MCFT. Vector2 includes second order effects such as compression softening, tension

stiffening and shear slip along crack surfaces of the reinforced concrete element. Analysis capabilities of the program are as follows, modeling rehabilitated structures and bond slip mechanism with reinforcement and concrete. Addition to these capabilities, loading sequence could be generated. By Vector2, 4-node rectangular or quadrilateral elements which have eight degrees of freedom (8 d.o.f), 3-node triangular element (6 d.o.f) and 2-node truss bar element (4 d.o.f) can be generated while meshing. 2-node bond link element and 4-node contact element are used for bar slip and adhesion.

1.3.1. Modified Compression Field Theory

The Modified Compression Field Theory was developed by Vecchio and Colins (1986). The constitutive relations were derived from the experimental testing of thirty reinforced concrete panels. These panels were subjected to pure shear and combination of shear and axial loads. From the test results, equilibrium, compatibility, and stress-strain relationships were formulated in terms of average strains and stresses. Equilibrium conditions control the balance of the externally applied loads to the internal element forces. Compatibility checks the agreement between deformation in concrete to an identical deformation in the reinforcement. And also, constitutive relationships for cracked concrete and reinforcement were formulated in terms of average strains and stresses.

MCFT considers cracked reinforced concrete as an orthotropic material. It is assumed that cracks can rotate or are freely reoriented. These cracks remain coaxial with the changing direction of the principal compressive concrete stresses. Characteristic compressive strength of the cracked concrete is decreasing (compression softening) when the large transverse tensile strains occur. After cracking, tensile stresses may continue in crack patterns due to the bond interactions between concrete and reinforcement. This phenomenon is known as tension stiffening. Concrete tensile strength decreases from characteristic tensile strength level as concrete tensile strain increases. The Modified Compression Field Theory (MCFT) proposes the above mentioned relationships.

Local failure mechanisms are considered with yielding of the reinforcement, fracture of the reinforcement at cracks or sliding shear failure along cracks. MCFT limits the local stresses at the crack and the average concrete tensile stresses to overcome these possibilities.

1.4. Objective of The Study

The purpose of the study relies on the effect of infill walls which avoid a collapse, or decrease the damage to the structure during an earthquake. The fundamental aim of the study shows the contribution of the lateral load capacity of the wire meshed infilled RC frame under reverse cyclic loading. This strengthening technique can be optimal in terms of ease to use and due to its low cost. It shortens retrofit time and occupants of the building do not need to be relocated. Furthermore, architectural design of the structure would not be altered. Besides there will be a minor increase in the mass of the building.

In the current work, the span length of the RC frame is 3150 mm and the height of the RC frame is 2250 mm. The columns and beams are 250 mm by 500 mm. The thickness of the clay infill wall is 190 mm. Four kinds of FE model and two different wall retrofitting techniques were utilized. All models were loaded under reverse cyclic loading. Firstly, a bare RC frame which is named as A0 was generated. It was used as control model. Then, model A0 was infilled with clay brick and was renamed as A1. Model A1 had been loaded under reverse cyclic loading. After the first reverse cycling, the model was strengthened with the wire mesh and loaded again. The new model was called A1R model. B1 and B2 models were the same as the A1 model and initially strengthened with wire mesh before loading. The wire mesh was clamped to RC frame in different diameters. The B1 and B2 models were strengthened with 3 mm and 6 mm wire mesh, respectively. C1 and C2 models were the same as the B models but they were rehabilitated with wire mesh, which was not clamped to the RC frame. Distribution of the wire mesh is 75 mm vertically and horizontally in the infill wall layer.

CHAPTER 2

A CORROBORATION STUDY OF VECTOR2

2.1. Introduction

An examination was undertaken using the program, VecTor2. It is a two-dimensional nonlinear finite-element program for reinforced concrete membrane elements based on the Modified Compression Field Theory (MCFT). The examination was intended to validate numerical model results of Vector2 against the computational results. Numerical model results were obtained from the finite element model of the RC beam and the column of the RC frame. Computational model results were obtained by utilizing the Modified Kent-Park Model and Hognestad Model. Confinement effects were not neglected due to the presence of the transverse reinforcement. For that reason, the Modified Kent-Park Model (confined) was utilized. Numerical model results were compared with computational results in terms of moment-curvature and moment-displacement values.

2.2. Computational Study of The RC Frame

The moment capacity and curvature of the cross-section for a determined rectangular reinforced concrete cross-section were computed by Scilab, a matrix-based software for technical computing. While calculating, a compatibility equation was adopted between the concrete and the reinforcement. Similiar compressive and tension strain was assumed between concrete and reinforcement which remains elastic. An initial compressive strain of concrete was determined and then a neutral axis was assumed. Reinforcement strains were found from the compatibility relation of similar triangles of strains. The tension and compression reinforcement's stresses were obtained according to ductile steel stress-strain response model.

Simultaneously, the compressive concrete stress was calculated by summation of the area below the Modified Kent-Park curve. This compressive stress was applied along the assumed neutral axis and along the width of the determined rectangular cross-section. The equilibrium equation was the sum of the horizontal stresses. The horizontal stresses consisted of tension or compression reinforcement of steel stress and compressive concrete stress. The equilibrium state is shown in Figure 2.1 and 2.2 and the compatibility and equilibrium equations are given in Eq. 2.1 to 2.3.

$$\frac{\varepsilon_{ci}}{\varepsilon_{s2}}=\frac{c}{c-d} \quad ; \quad \frac{\varepsilon_{ci}}{\varepsilon_{s1}}=\frac{c}{h-c-d} \quad compatibility\,equation \qquad (2.1)$$

$$F_{total}=F_{ci}+F_{s1}+F_{s2}=0 \qquad equilibrum\,equation \qquad (2.2)$$

$$F_{ci}=\Sigma\,\sigma_c b_w c_i \quad ; \quad F_{si}=A_{si}\sigma_{si} \qquad (2.3)$$

Unless the equilibrium equation was satisfied, a new neutral axis should be assumed until this process was accomplished. If this loop was done from the initial compressive strain to the ultimate concrete compressive strain, the moment capacity of the determined cross-section for each compressive strains were calculated.

The curvature of rectangular reinforced concrete cross-section was computed due to the obtained compressive concrete strains and the determined neutral axis. The curvature of the rectangular reinforced concrete cross-section is the division of the compressive concrete strain to neutral axis depth. The schematic view of compatibility and equilibrium conditions are shown in Figure 2.1. As seen from the figure, the tension stress of the concrete was neglected (Ersoy 2001).

The cross-section of the rectangular column was 500 mm in depth and 250 mm in width. The column length was 2250 mm. The compression and tension reinforcement areas were 615.7 mm². The ratio of the transverse reinforcement is 0.002. The concrete cover was 62.5 mm in thickness. The peak uniaxial compressive stress of the concrete was determined as 14 MPa. The yielding stress of the steel is 420 MPa with a yielding stress of 0.002 strain.

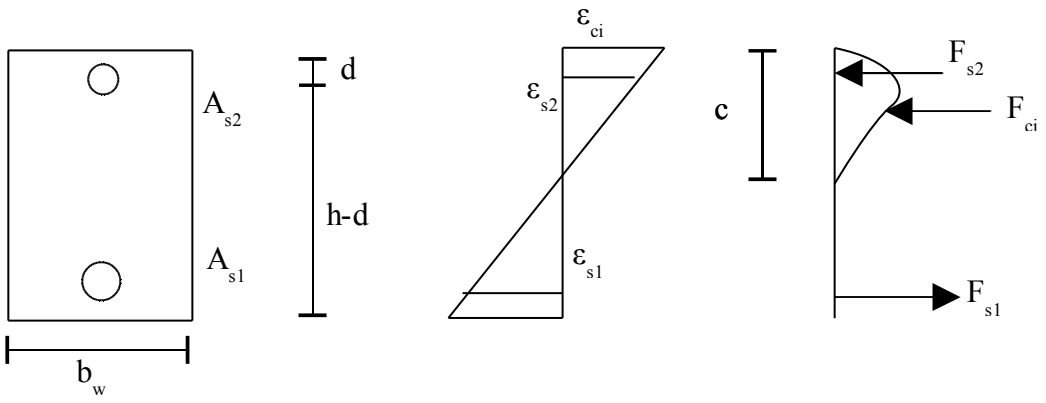

Figure 2.1. Cross-section of the models and compatibility and equilibrium conditions

In the computational study, the bending rigidity of the top beam of the RC frame model was assumed infinity. Thus the total moment of the column of the RC frame was zero at the half length of the column. This situation brought out to measure the half displacement of the RC frame. At the current point of the study, it was possible to calculate the relative displacement of the column by computing the moment-curvature curve. The relative displacement was calculated by taking the moment of the area below the moment-curvature curve with respect to the midpoint of the column. The Scilab file of the computational study is given in Appendix A1.

2.3. Analytical Study of The RC Frame

The reinforced concrete frame model was generated. The column which was a member of the RC frame had similar cross-section dimensions and reinforcement as in the computational model. The span of the RC frame was 3650 mm. The top of the RC frame was subjected to monotonic lateral displacement loading. 1 mm of prescribed displacement was applied to the top of the beam. At each loading stage, 0.5 mm loading increments were applied to the top of the beam until flexure failure occurred. The material properties were matched in most situations ?? and also some were identical compared to computational study.

In addition to the above mentioned facts, little differences were obligatory while analyzing the RC frame. The Young Modulus of the top beam was 18708 MPa and its moment of inertia was $2.6x10^9$ mm^4 whereas the computational model assumed that the beam had infinitive bending rigidity. 8 mm diameter bars were used in beams and columns with a minimum transverse reinforcement ratio of 0.2 percent. The peak uniaxial compressive stress of the concrete was designed as 14 MPa. The yielding stress of the steel was 420 MPa with a yielding strain of 0.2 percent. The ultimate strength of the steel was 500 MPa with an ultimate strain of 2.2 percent. Normally the ultimate strain of the steel was 0.012.

The differences were seen in stress calculations after the yielding phase of the steel bar. In the computational part it was assumed that there would be no rupture on the steel bar if the computed strain was over the hardening strain.

The analysis were performed using the program Vector2.The RC frame was meshed for finite element analysis. Rectangular elements (8 d.o.f) were used for the beams and columns of the RC frame. All longitudinal reinforcements were modeled as truss bar elements (4 d.o.f). All stirrup steels were modeled as smeared reinforcement (0 d.o.f). The mesh of the RC frame, loading points and support conditions are given in Figure 2.2.

The moment capacities and the shear forces of the bottom and top joints of the column should be computed for each load stage with respect to the displacement of the column. For comparison purposes, the recorded displacement shall be chosen at the zero moment location in the column. And it is known that this location can change depending on the loading, non-linearity, and symmetry of the model. In order to determine the cross-sectional moment that is equal to zero, the stress of the steel reinforcement and discretized rectangular concrete elements were found for each load stage. Ones the stresses were found, the moment and shear force resistance of these sections were found. This step was repeated over the column height, until the zero-moment location was found. Then the relative displacements of the column were measured at these calculated heights. At the end of one step, one data point of moment vs. displacement was calculated.

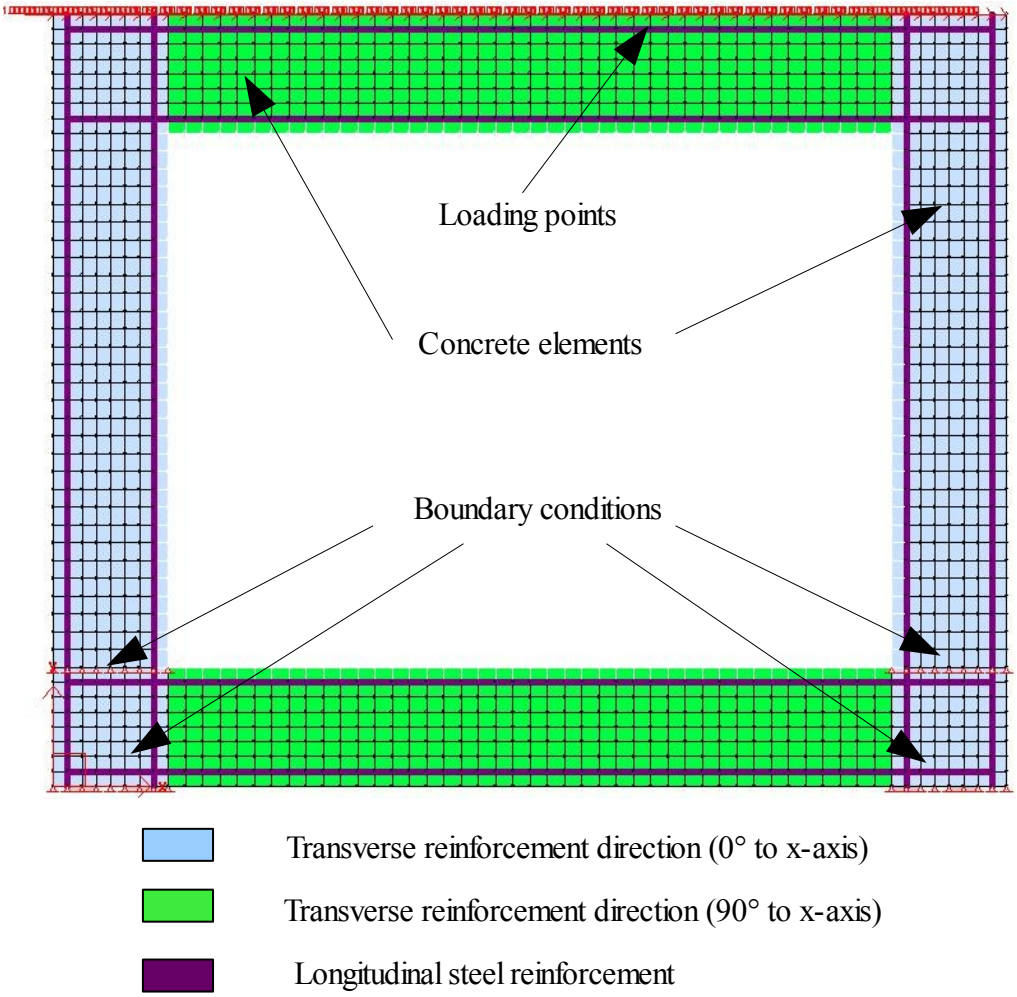

Figure 2.2. The mesh of the RC frame and loading points

Table 2.1. summarizes the material properties for the concrete elements, reinforcement elements, bond elements and the corresponding analytical models that were chosen for each material properties in Vector2. These analytical models are used for the computation of the response of the each elements under the given loading conditions. For several material properties, there were multiple analytical models. These properties will be discussed widely in chapter 4.3.5.

Table 2.1. Analytical models of the RC frame used in the FE analysis

Material Property	Analytical Model
Concrete	
Concrete Compression Pre-Peak Response	Hognestad (Parabola)*
Concrete Compression Post-Peak Response	Modified Park-Kent *
Concrete Compression Softening	Vecchio 1992-A (e1/e2-Form)*
Concrete Tension Stiffening	Bentz 2003*
Concrete Tension Softening	Linear*
Concrete Tension Splitting	Not considered*
Concrete Confinement Strength	Kupfer / Richart Model*
Concrete Lateral Expansion	Variable - Kupfer*
Concrete Cracking Criterion	Mohr-Coulomb (Stress)*
Concrete Crack Slip Check	Vecchio-Collins 1986*
Concrete Crack Width Check	Agg./5 Max Crack Width*
Concrete Creep and Relaxation	Not Available*
Concrete Hysteretic Response	Nonlinear w/ Plastic Offsets
Reinforcement	
Reinforcement Hysteretic Response	Seckin Model (Bauschinger)*
Reinforcement Dowel Action	Tassios Model (Crack Slip)*
Reinforcement Buckling	Asatsu Model*
Bond	
Concrete Bond	Perfect Bond

* Default model

The moment-displacement relation of the column calculated from the finite element analysis of the RC frame was compared to the computational results in Figure 2.3. Before the yielding point the moment of the analytical study was overestimated compared to the computational study. This was due to the fact that tension stresses of the concrete were neglected in the computational study (Modified Kent-Park Model). After cracking of concrete, the concrete tensile stresses decreased and the moment capacity of the column was descending.

When tension stresses of the concrete reached the characteristic tension stress of the concrete, the member started to crack. As a result, the member stiffness decreased and was almost constant up to the yield point. For that reason, the calculated behaviour

of the moment-displacement responses was unlike up to yield point of the reinforcement. The analytical model had a moment capacity of 9.49 t-m whereas the computational one had a capacity of 9.01 t-m at the yielding point. At the yielding point the relative displacement of the computational model and of the analytical model were equal to each other.

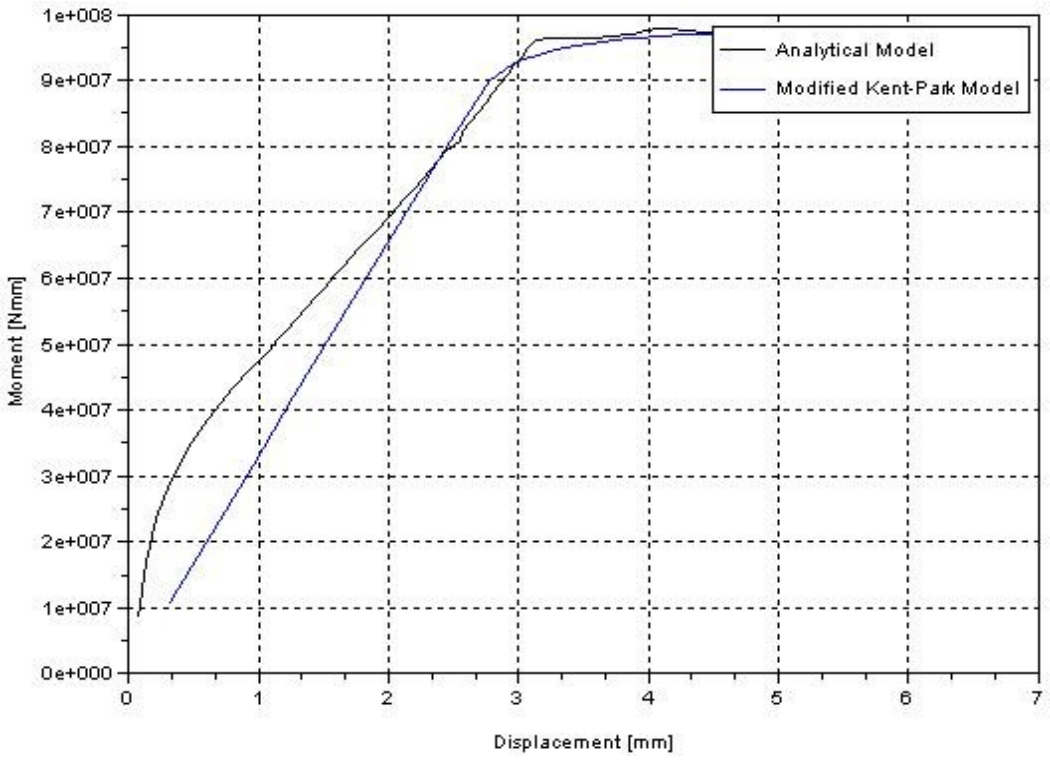

Figure 2.3. Comparisons of moment-displacement

2.4. Discussion of The RC Frame Results

The behaviour of both models under flexure were similar in terms of the relationship between the moment and displacements after the yield point. Some discrepancy were seen in the magnitude of the moment capacity and displacement at the yield point. Some of the factors played a leading role at divergence. For instance, usage of tension stresses gave additional moment to column and caused extra moment capacity to the column in the analytical study. The strain-displacement curve of the

cross-section remained linear n every load stage in the computational study and this was different in the analytical model. The correct modes of failure and crack patterns were captured with Vector2 from Figure 2.4.

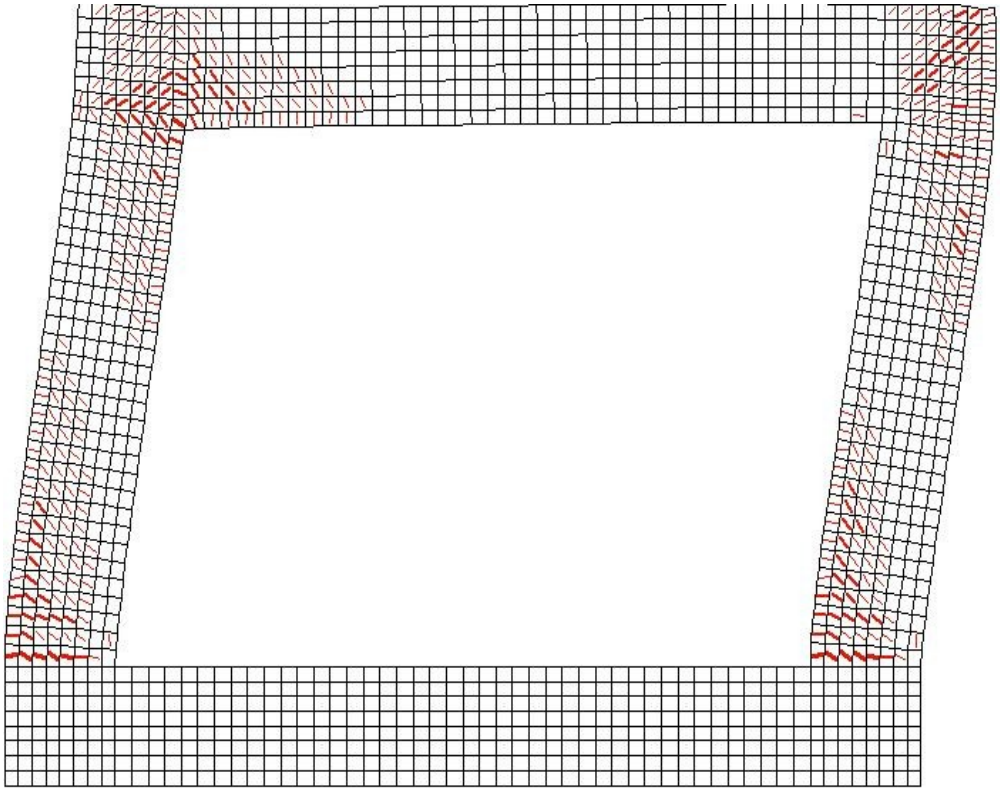

Figure 2.4. Crack patterns of the RC frame

CHAPTER 3

EXPERIMENTAL TESTING OF CLAY BRICKS

3.1. Introduction

The purpose of this chapter is to investigate the compressive strength of hollow clay bricks that were used to form the infill wall. The details of the experimental program, including the properties of the hollow clay brick specimens, test setup, instrumentation and the loading sequence are discussed in this chapter. The testing was conducted by the use of compressive testing machine UTM-4000, which has a capacity of 600kN. It is a computer controlled system that reads the stroke from the head together with the applied load and time. The results of these tests comprised the compressive strength values of the clay bricks. In the following parts, the obtained values were used in the (NLFEA) program, Vector2.

3.2. Test Specimens

Eleven hollow clay bricks were collected from different construction sites as test specimens for the experimental work. Their size were determined from the general usage in the brickworks of any construction. The dimensions of the selected specimens were 135 mm in height, 190 mm in width and 190 mm in length. Bricks that had macroscopic defaults such as burnt clay, fractured surfaces or inadequate geometric orthogonality of holes were not considered.

The test specimens were tested at Umutlab Laboratory which is approved by the Ministry of Public Works and Settlement. The dimensions of the test specimens were varying. All the test specimen provided the minimum size requirements specified by the

Turkish Code of Horizontal Coring Bricks for structural walls (TS 4563, 1986). The specimens were measured by a metric compass as seen in Figure 3.1. The thickness of the test specimens were determined by taking three measurements at the center holes and four measurements near the edges. The average thickness, width and length of the specimens were used to calculate the net area. The first set of the specimens, which were loaded in the vertical direction to the holes are prefixed by asterix " * ".

Figure 3.1. Measurement of the test specimens

3.3. Test Setup

The testing equipment was prepared before the tests. The surfaces of the brick specimens and bearing faces of the compressive testing machine were cleaned. Test specimens were placed on the lower bearing block by aligning their centroidal axes to the center of the bottom block of the machine. The soft wooden spacers were placed on the bearing faces of the test specimens as a remedy against the surface defects of the test specimens. These procedures prevented any undesired point loading. The first and second set of the specimens before loading is shown in Figure 3.2 and Figure 3.3.

Figure 3.2. Test specimen of set1

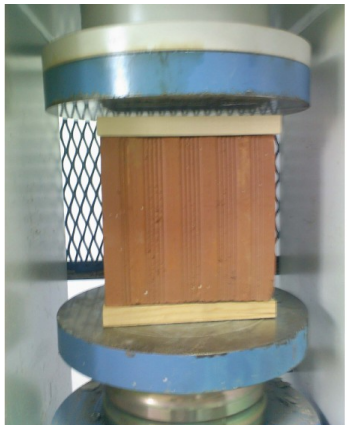

Figure 3.3. Test specimen of set2

3.4. Loading Sequence

The test specimens were loaded in parallel and vertical directions with respect to brick holes. The rate of the loading was changing related to the expected capacity of any test specimen. According to loading procedures of hollow clay brick standards, the loading duration should not be less than one minute, and no more than two minutes. The loading rate was selected as 1.2 mm/minute to 1.8 mm/minute (Bodycote 2008).

3.5. Material Poperties

The average ratio of the net area to the gross area of the clay bricks was 30%. The average compressive strength of the hollow clay bricks which was loaded in vertical and parallel direction were 5.5 MPa and 6.86 MPa, respectively. The properties of the test specimens are given in Table 3.1.

The experimental results exhibited a wide range of compressive strength values. The compressive strengths of the first set of specimens which were loaded vertical to the direction of holes have a mean value of 5.58 MPa and the data changed from 3.52

MPa to 7.42 MPa. This corresponds to a 37% change from the mean value. The brittle and sudden failure of samples were observed as shown in Figures 3.4. and 3.5. Contrary to first set, the second set of specimens which were loaded parallel to the direction of holes, seemed more stable than the first group in terms of the distribution of the compressive strength values. Their compressive strengths ranged from 5.43 MPa to 6.84 MPa, except for the one with a strength value of 9.86 MPa. These specimens possessed more strength than the first group, due to the same direction of the test bricks holes and loading directions.

Table 3.1. Properties of the test specimens

Test Specimens	Size (mm^3)	Net Area (mm^2)	Unaxial Load (N)	Compressive Strength (MPa)	Loading Sequence (mm/min)
*1	185x185x130	7400	47010	6.35	1.2
*2	185x185x133	7400	52000	7	1.4
*3	185x183x130	6954	51600	7.42	1.8
*4	186x186x133	7068	28020	3.96	1.7
*5	186x183x130	6882	35190	5.11	1.7
*6	189x189x133	7182	25560	3.55	1.6
7	186x186x135	7068	39900	5.64	1.6
8	186x186x135	7068	44620	6.31	1.6
9	185x185x130	7400	40240	5.43	1.55
10	183x183x130	6954	68600	9.86	1.5
11	185x185x130	7400	50800	6.86	1.6

Note: (*) Vertically loaded

Figure 3.4. Test specimen of set1 after loading

Figure 3.5. Test specimen of set2 after loading

3.6. Discussion of The Experimental Results

Loading sequence and unidentified design classifications were the most common factors that had influence on the test results. During the loading history of the test, some cracking sounds were perceived. At that time instance of the loading, the possible failures and the brick's compression strength should be determined by increasing the load to a maximum level which can be sustained by the brick (US Army Corps of Engineers 2008).

3.7. Limitations & Errors

Some problems occurred due to the impossibility of gaining experience in testing of clay bricks because of time constraint and due to the lack of knowledge about the classification of different kinds of manufactured bricks. These factors influenced the loading speed and the evaluation of the test specimens material properties under uniaxial loading.

Testing facilities of the study were limited due to some important facts. Most of the test equipments and machines in the Umutlab Laboratory were applicable to

concrete samples. A time limitation always existed during the tests because of the professional activities of the Umutlab Laboratory. If the Laboratory of the Civil Engineering Department would have been used, limitation on time had disappeared. Additionally more comprehensible results would have been obtained by utilization of calibrated testing machines and by means of sufficient number of tested samples. Repetition of these testing procedures had possibility to overcome the errors that came from time duration of the loading sequence. These repetitions will result in more realistic estimation of compressive strength and leads to gain experience on the conducting data of the test experiments. Not only compressive strength but also the modulus elasticity of the test specimens could be computed in the Laboratory of The Civil Engineering Department.

Infill walls generally were made of bricks and mortar. These masonry units were influenced by the properties of the bricks and mortar. Various size of masonry prisms would have been tested if the testing conditions were well suited. The strength and modulus of elasticity of the masonry units under compression could not be done due to the inadequate length and width of the bearing blocks of the test machine. For that reason, only hollow clay brick properties were used instead of infill wall in the finite element analyses.

For rehabilitated structures, it is suggested that the modulus of elasticity and the compressive strength of the hollow clay brick prisms that are formed as the bearing infill walls could be taken as 1000 MPa and 1 MPa, respectively (Turkish Earthquake Code 2006).

CHAPTER4

FINITE ELEMENT ANALYSIS OF A REINFORCED INFILL WALL

4.1. Introduction

The aim of the finite element analysis was to see the effects of the rehabilitated reinforced concrete (RC) frame together with the wire meshed infill wall. This was accomplished by using a finite element software that has an integrated concrete and masonry material model. The software, Vector2, was used in this analysis. Models were generated and then the improvement on the strengthening in terms of energy dissipation, lateral load capacity was investigated. The modeling procedure and assumptions together with the analytical results were discussed in the current chapter.

Section 4.2 presents the finite element implementation of the program. Section 4.3 contains the descriptions of the modeling technique. The analysis results of the model under reverse cyclic loading are described in Section 4.4. Finally, Section 4.5 presents the discussion of the results of all FE analysis.

4.2. Finite Element Algorithm

Vector2 is a program that utilizes the Modified Compression Field Theory (MCFT) with a rotating smeared-crack model for modeling reinforced concrete (Vecciho 1986). The Vector2 algorithm for nonlinear finite element analysis was summarized by the flow chart in Figure 4.1.

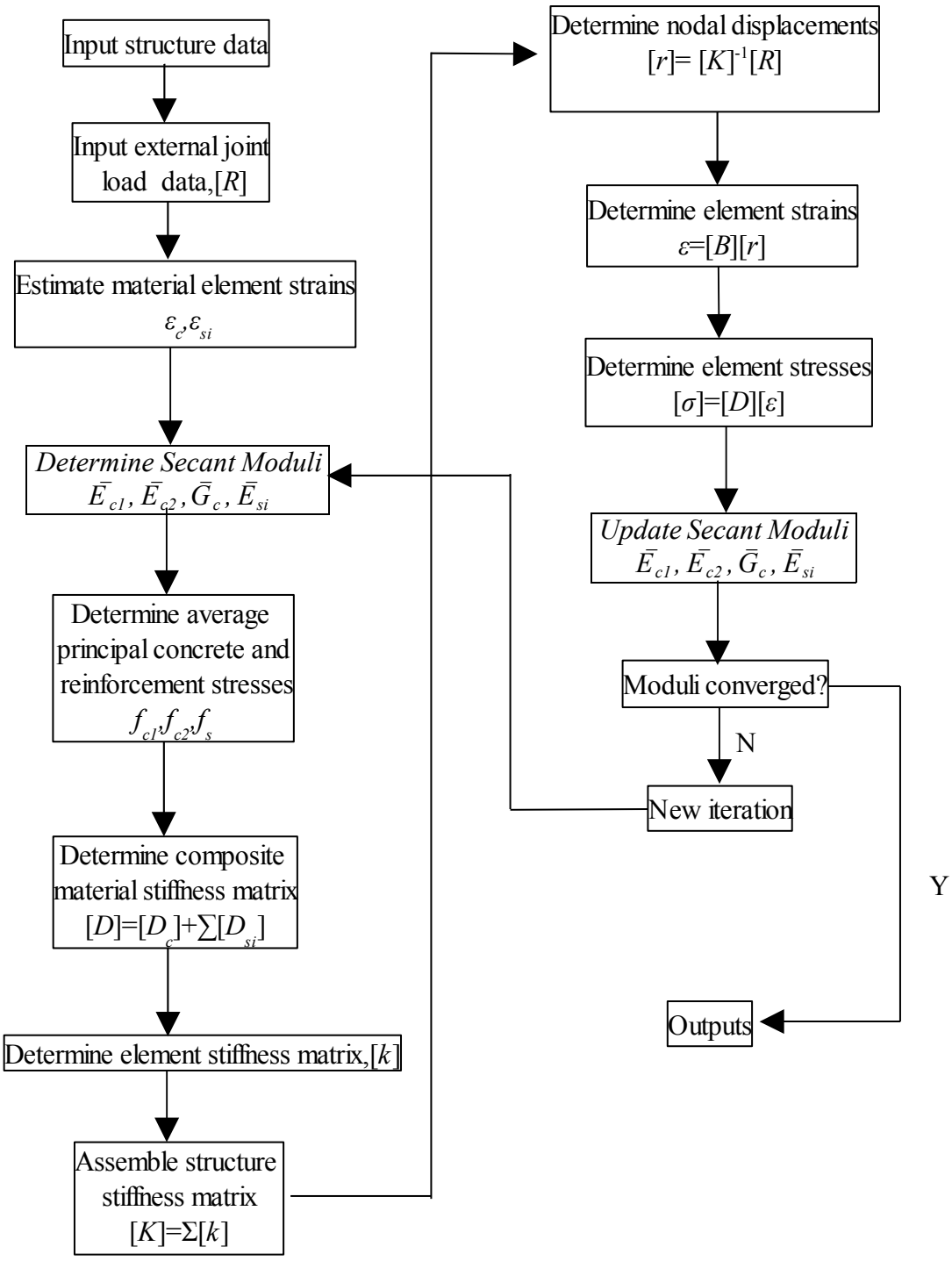

Figure 4.1.Vector2 finite element analysis algorithm

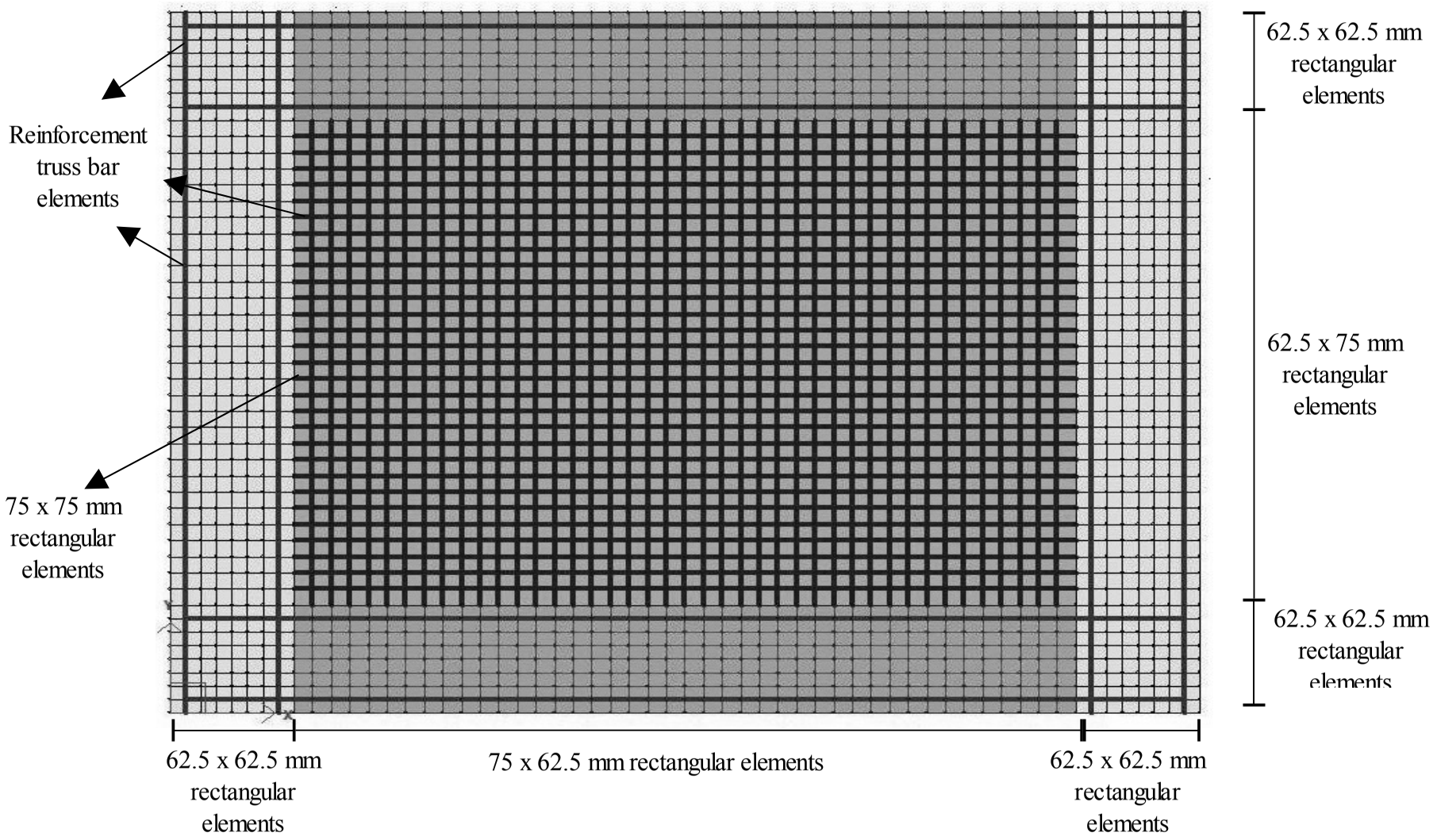

Figure 4.2. FE mesh

4.3. Finite Element Modeling with Vector2

The FE mesh was built by using the program FormWorks. It is a pre-processor program that is suitable for Vector2. The definition of FEM models are given below in Table 4.1.

Table 4.1 The definition of FEM models

A Series
A0= bare RC frame (control model)
A1= A0+ infill wall
A1R= A1 + 6 mm wire mesh installed after 1.cycle (clamped to RC frame)
B Series
B1= A1+ 3 mm wire mesh (clamped to RC frame)
B2= A1+ 6 mm wire mesh (clamped to RC frame)
C Series
C1= A1+ 3 mm wire mesh (clamped to infill wall)
C2= A1+ 6 mm wire mesh (clamped to infill wall)

Rectangular elements were utilized to model the concrete. The longitudinal reinforcement and steel wire mesh were modeled by truss bar elements. The resulting finite element mesh is presented in Figure 4.2.

4.3.1. Concrete Elements

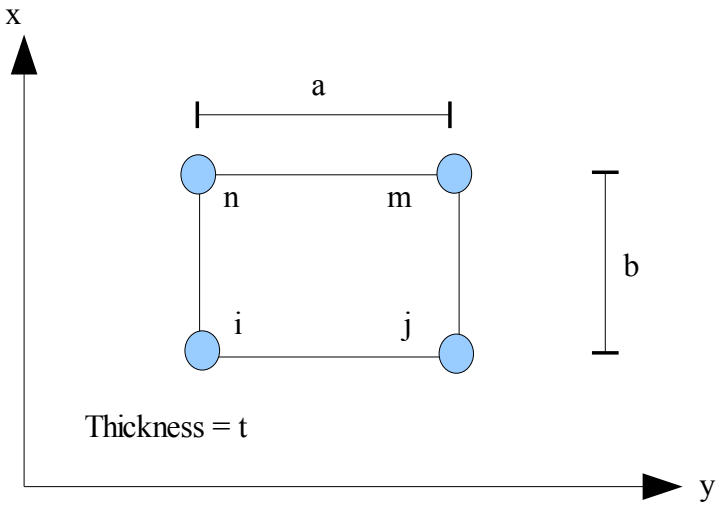

Figure 4.3. Plane stress rectangle element

Plane stress rectangular elements (see Figure 4.5) with a uniform thickness, *t*, were used to model both reinforced and unreinforced concrete. An optimal meshing was created due to the limited number of nodes and elements that can be visualized by the post-processor Augustus. The size of the rectangular elements at the beam-column connections were 62.5 mm x 62.5 mm to coincide with the depth of the longitudinal reinforcement. The size of the rectangular elements at the columns and beams were 75 mm x 62.5 mm to coincide with the longitudinal reinforcement depth and wire mesh distribution. 75 mm x 75 mm rectangular elements were used as plain concrete material to represent infill wall. Well-distributed transverse steel reinforcement was modeled in beams and columns. Three different reinforcement concrete types were used. They were varying according to different reinforcement ratios and cylinder strengths as seen in Table 4.2. Concrete types 1 and 2 were assigned to the typical reinforced concrete beam and column sections, respectively. Concrete type 3 was a unreinforced concrete element which was assumed as an infill wall. The concrete type assignment regions are viewed in Figure 4.4.

Table 4.2 Concrete element types

Concrete Type	Location	Thickness (mm)	Smeared Reinforcement			Concrete Cylinder Strength (MPa)
			Diameter (mm)	Direction (°)	Ratio %	
1	Column	250	8	0	0.2	14
2	Beam	250	8	90	0.2	14
3	Infill wall	190	-	-	-	1

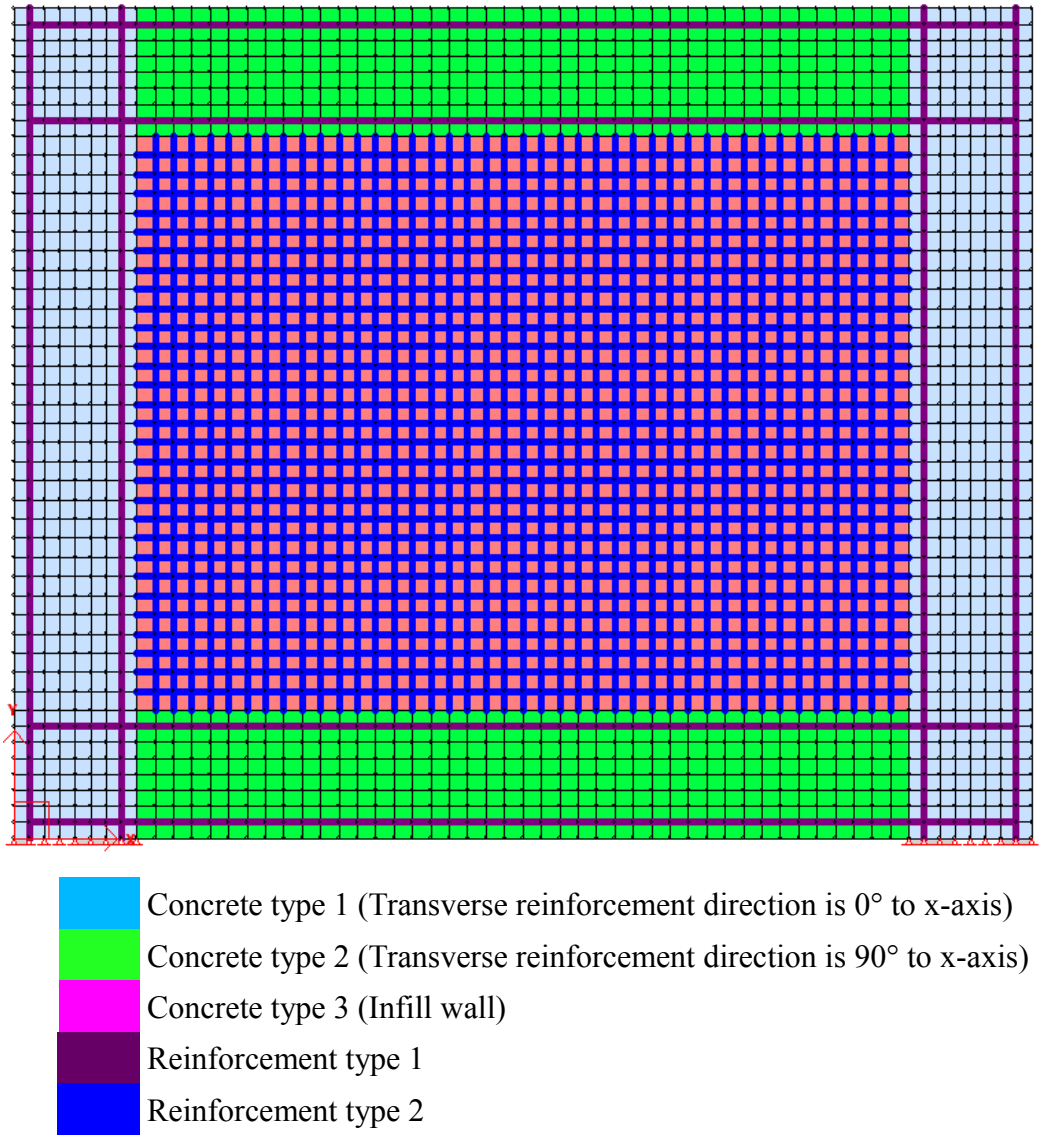

Figure 4.4. Material assignment

4.3.2. Reinforcement Elements

Ductile steel reinforcement and wire mesh were modeled using discrete truss elements. Truss elements are two-node elements with a uniform cross-sectional area as shown in Figure 4.5. Each node has two degrees of freedom in x and y directions. Figure 4.4. shows the assigned reinforcement locations.

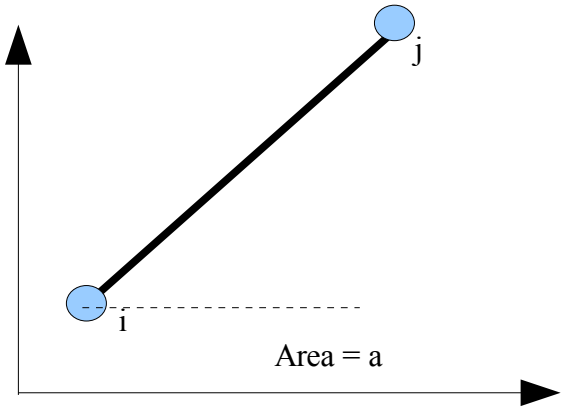

Figure 4.5. Truss bar element

Ductile steel truss bar elements were used as longitudinal reinforcements in the beams, columns and wire mesh reinforcements on the surface of the infill wall. The length of each truss element would be either 62.5 mm or 75 mm depending on the nodal geometry. The nodal geometry was governed by the distribution of the rectangular elements. A total number of 2856 bar elements were used in B Series and or 2716 truss bar elements were used in C Series. 416 truss bar elements were used within the reinforced concrete, and the rest of the truss bar elements were used for strengthening the infill wall. Table 4.3. summarizes the types of the truss bar elements.

Smeared stirrups were designed with the minimum reinforcement ratio according to Turkish design code (TS 500). It was aimed to see the shear strength contribution of the infill and wire mesh thus the shear capacity of the columns of the models were assumed minimum. Perfect bond was assumed between the concrete elements and reinforcement elements. Figure 4.4. shows the reinforcement type properties and assigned locations.

Table 4.3 Reinforcement element types

Reinforcement type	1	2
Location	beam/column	infill
Direction	longitudinal	vertical & horizontal
Diameter (mm)	28	3/6
Yield strength (MPa)	420	420
Young modulus (MPa)	200000	200000
Ultimate strength (MPa)	500	500
Strain hardening strain (%)	0.01	0.01

4.3.3. Support Conditions

In order to represent the actual movement of a RC frame at a story level, the nodes at the bottom layer of the lower beam were not restrained in x and y directions. Thus the frame could rotate at a story level. On the other hand, the nodes at the bottom layer of the columns were fixed against displacements in the x and y direction as seen in Figure 4.6.

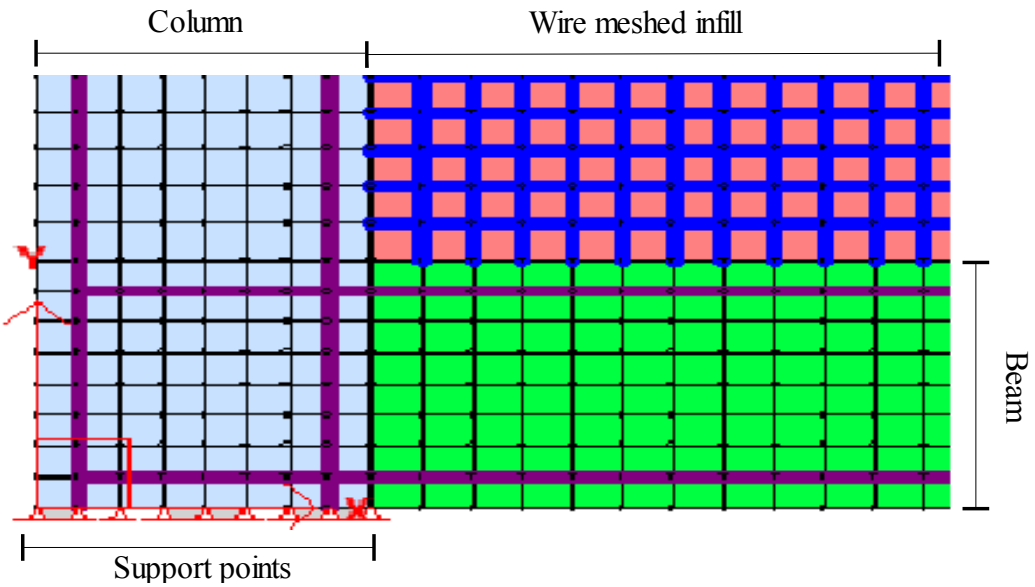

Figure 4.6. Support conditions

4.3.4. Loading Procedures

In the FE model, fifty nine nodes of the top beam were assigned an initial value of 1mm prescribed displacement in the x direction. The displacement increment was maintained by 0.5 mm displacement factor throughout each load stage. The prescribed displacement was changing at every increment of the analysis. Reverse cyclic loading type was assigned for all analyses . An example of reverse cyclic loading was viewed in Figure 4.7. The direction of the nodal displacements was replacing at every reverse half cycle. This procedure continued until the last stage of the prescribed displacement value given in the job file. The applied prescribed displacements were shown at the top of Figure 4.8.

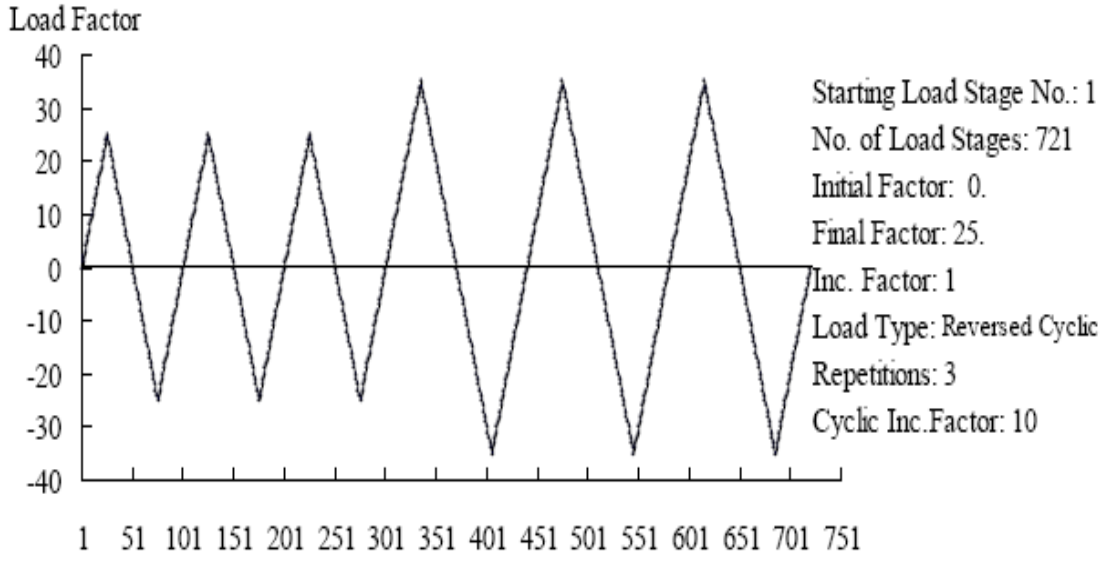

Figure 4.7. Reverse cyclic loading
(Source: Vector2 and Formworks User's Manual 2002)

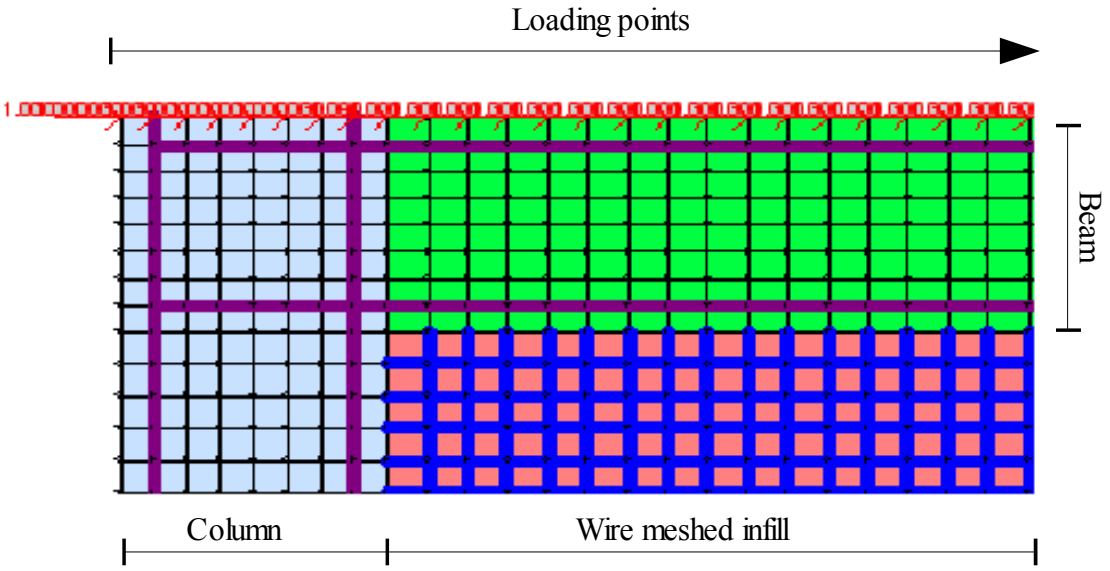

Figure 4.8. Assigned prescribed displacement

4.3.5 Concrete, Reinforcement and Bond Analytical Models

From the Vector2 & Formworks User's Manual, the description of the all analytical models for different materials were presented. Adding to these models, there were extra analytical models such as concrete crack width check, reinforcement dowel action, and concrete bond model.

The analytical models described the constitutive and behavioral attitudes of the response of the concrete and the reinforcement material. Further details of the analytical models can be investigated in the Vector2 & Formworks User's Manual.

For the concrete compression pre-peak response, the default Hognestad Parabola was chosen to reflect the relatively normal concrete strength that were used in the analyzed models.

For the concrete compression post-peak response, the default Modified Park-Kent model was selected to answer for the enhancement of concrete strength and ductility due to confinement.

In cracked concrete, compression softening is the reduction of compressive strength relative to the uniaxial compressive strength due to coexisting transverse cracking and

tensile straining. Vecchio 1992-A (e1/e2-Form) analytical model was selected to avoid overestimation of the softening effect when the principal tensile strains are very large such as the yielding of the reinforcement.

Tension stiffening is known as decreasing average stress-strain response of concrete in tension. Due to bond action with the reinforcement, average concrete tensile stresses continue to exist in the concrete between the cracks and the interface of the reinforcement. Bentz model proposed a tension stiffening formulation that incorporates the bond characteristics of the reinforcement and concrete.

Tension softening refers to the presence of post-cracking tensile stresses in plain concrete. The effects of concrete tension softening was important in lightly reinforced regions exhibiting brittle failure modes. By the fracture mechanics, a localized crack requires energy while the fracture process devolops and the crack widens. If the crack is relieved of stress, these actions lead the dissipation of energy. This property affects the ductility of the member. The linear model was the base curve descends linearly from the cracking stress at the characteristic strain to zero stress.

Confined concrete shows enhanced strength and ductility in compression. Kupfer/Richart Model proposes a determination between the triaxial strength of concrete subject to biaxial compression.

Due to internal micro cracking, the rate of the lateral concrete expansion increases as the compressive stress increases. Variable Poisson's Ratio – Kupfer Model determines that the Poisson’s ratio increases nonlinearly as compressive strain increases.

The cracking strength generally decreases as transverse compressive stress actions increase. Mohr-Coulomb (Stress) Model is assumed that the concrete is ductile to redistribute stresses along the failure plane. The failure envelope is tangent to the Mohr’s circles which is defining the combinations of shear stress and normal stresses in shear failure.

It is necessary to check the local shear stresses at a crack not to exceed a maximum shear stress corresponding to sliding shear failure. Vecchio-Collins 1986 Model proposes a relationship on limitation of increasing shear stress while the uniaxial concrete cylinder compressive strength increases or the crack width decreases or the maximum aggregate size increases.

The crack width check model maintains to reduce average compressive stresses when crack widths exceed a specified limit to prevent tensile strains, which may create additional softening. Secondly, to prevent overestimation of principal stresses due to the transmission of local compressive stresses across the crack.

The hysteretic response of concrete played an important role to the strength and ductility of the structures under reverse cyclic loading (Palermo and Vecciho, 2006). Nonlinear with plastic offsets model was selected to describe how concrete reloads and unloads from the monotonic concrete stress-strain curve of the reinforced concrete structures subjected to cyclic or reverse cyclic loading. The hysteretic loops, are indicative of the internal damage and energy dissipation under cyclic loading.

Ductile steel reinforcement model was selected for the stress-strain response of the reinforcement materials. It consists of a linear-elastic response with a yield plateau, and a linear strain-hardening phase until rupture.

Hysteretic response model of the reinforcement describes the reloads and unloads from the monotonic stress-strain curve. It includes the Bauschinger effect, in which the reinforcement shows premature yielding upon load reversal after plastic prestraining due to stress changes.

Dowel action helps shear resistance with reinforcing bars as the bars were crossing a crack transversely to the axis of the reinforcement. In some circumstances; small amount of transverse reinforcement's dowel action may contribute to the shear strength and post-peak ductility of reinforced concrete members. Tassios Model gives dowel force-displacement relationship which is modeled as elastic-plastic.

Asatsu Model is selected for buckling failures. When reinforcement is located near the surface of a concrete member and subjected to high levels of compressive stress, bar buckles. The associated concrete cover and reinforcement contribute to the flexure and shear resistance of the member.

Perfect bond model was assumed between the bar and concrete element to prevent deformation of the bond element. Summation of the material properties for the concrete elements, reinforcement elements, bond elements, and the chosen analytical models for each material were shown in Table 4.4.

Table 4.4. Analytical models used in the FE analysis

Material Property	Analytical Model
Concrete	
Concrete Compression Pre-Peak Response	Hognestad (Parabola)*
Concrete Compression Post-Peak Response	Modified Park-Kent *
Concrete Compression Softening	Vecchio 1992-A (e1/e2-Form)*
Concrete Tension Stiffening	Bentz 2003*
Concrete Tension Softening	Linear*
Concrete Tension Splitting	Not considered*
Concrete Confinement Strength	Kupfer / Richart Model*
Concrete Lateral Expansion	Variable - Kupfer*
Concrete Cracking Criterion	Mohr-Coulomb (Stress)*
Concrete Crack Slip Check	Vecchio-Collins 1986*
Concrete Crack Width Check	Agg./5 Max Crack Width*
Concrete Creep and Relaxation	Not Available*
Concrete Hysteretic Response	Nonlinear w/ Plastic Offsets
Reinforcement	
Reinforcement Hysteretic Response	Seckin Model (Bauschinger)*
Reinforcement Dowel Action	Tassios Model (Crack Slip)*
Reinforcement Buckling	Asatsu Model*
Bond	
Concrete Bond	Perfect Bond

* Default model

4.4. Finite Element Analysis

The span length of the RC frame models were 3150 mm and the height of the RC models were 2250 mm. All the columns and beams had a dimension of 250 x 500 mm with 1 % of longitudinal reinforcement ratio. Transverse reinforcement ratio of the columns and beams were equal to 0.2 %. Concrete strength was 14 Mpa which was simulating low strength concrete quality in Turkey. The reinforcement had a yield strength of 420 Mpa and a ultimate strength of 500 Mpa. The infill walls were formed

of hollow-clay brick with a thickness of 190 mm and a compressive strength of 1 MPa.

In all series, reverse cyclic analysis were carried out. First analysis was conducted by neglecting the presence of the infill wall, named as A0 model. Secondly, A1 model was generated with a bare RC frame and infill wall, after the first cycle was fulfilled, the A1 model substituted into A1R repaired model. 6 mm diameter wire mesh was installed and activated for adding to infill in A1R model. Thirdly, the models in Series B, wire mesh was added in different diameters (3 and 6 mm) to the structure before the reverse cyclic loading. Series B models were different from Series C by the installation technique of the wire mesh to the RC frame. Two different installation techniques were used. In Series B, wire mesh was clamped to RC frame, whereas in the Series C, the wire mesh was left loose at the brick to R/C frame edge. Table 4.5. summarizes each type of element models that were used in the wall.

Table 4.5. Summary of the models used in the FE analysis

Element Types	Number of elements						
	Control	Series A		Series B		Series C	
	A0	A1	A1R	B1	B2	C1	C2
Concrete Type 1 (column)	736						
Concrete Type 2 (beam)	672						
Concrete Type 3 (infill wall)	_	1260					
Longitudinal Steel Reinforcement (28mm)	408						
Wire Mesh Steel Reinforcement (3 mm)	_	2440				2300	
Wire Mesh Steel Reinforcement (6 mm)	_						
Number of Nodes	1584	2773					

4.5. Analysis Results

The simulation results of the models were iterated with FEM program, Vector2. Three series of RC frame with a control model (A0) that were subjected to the prescribed reverse cyclic loading. Table 4.6. summarizes the lateral displacement and peak lateral loads for models of the analytical study. The comparisons of the lateral load and displacement of the models were illustrated from Figure 4.9 to 4.20.

Table 4.6. Lateral displacement and peak lateral loads of the models

	Peak Lateral load (kN) (forward cycle)			Peak Lateral load (kN) (reverse cycle)			Lateral displacement (mm)					
	1st cycle	2nd cycle	3rd cycle	1st cycle	2nd cycle	3rd cycle	1st cycle		2nd cycle		3rd cycle	
							F	R	F	R	F	R
A0	-91.4	-129.6	-164.6	89.8	128.4	164.1	5	-5	9.96	-10	14.94	-15
A1	-221.5	-193.3	-187.4	173.7	163.6	184.5	4	-4	9.94	-10	14.4	-15
A1R	-235.6	-281	-277.9	236	262.5	269.4	4.8	-4.9	8.44	-10	14.92	-15
B1	-228.1	-204.1	-225.2	181.8	202.9	209.7	3	-4.5	9.45	-10	14.4	-14.5
B2	-305.9	-326.2	-311.5	302.1	265.3	254	4.9	-5	5.97	-10	13.92	15
C1	-223	-157	-188	166	157.5	200.8	2.49	-4.48	9.95	-10	14.93	15.03
C2	-178	-174.9	-221	129.7	172.9	208.2	2.97	-3.49	9.95	-10	14.93	-15.02

4.5.1. Analysis Results of Series A

Model A1 showed greater energy dissipation and lateral load capacity than the A0 model because of the presence of the infills. Before the first diagonal shear crack at the infill, lateral load capacity of the model reached 157 kN. After a slight decrease in the load capacity, the frame regained the load capacity due to the occurrence of the compression zone between the opposite frame diagonals of infill. Then, the second diagonal shear crack was visualized. At the first forward cycle loading, a peak load of 221.5 kN was reached at around 4 mm, which was greater than the capacity of the A0 model. It reached a peak load of 91.4 kN at 5 mm. The damage modes of first forward cycle loading were similar to first reverse cycle loading. Again, diagonal shear crack was seen at the opposite diagonal of the frame at the load of 173.7 kN in A1 model. The second and third repetitions of reverse cycle loading was leading to shear crushing in the web and boundary of the infill in the model A1. The maximum average truss bar stresses were 382.7 MPa at the bottom of the exterior side of columns and smeared transverse reinforcement stresses were 331.40 MPa at the interior part of the column-beam joints. The maximum stresses of the concrete elements were 12.36 Mpa at the bottom of the columns.

A0 model reached the maximum load of 164.6 kN at 15 mm top displacement at the third forward cyclic loading whereas A1 model had lateral load of 187.4 kN at the same displacement. At this rate, the maximum average truss bar stresses were 384 MPa at the bottom part of the columns and smeared transverse reinforcement stresses were 332 MPa at the column-beam joints. The maximum stresses of the concrete elements were 12.61 MPa at the bottom part of the columns. Flexural and shear cracks were seen at the beam-column connections similar to the A1 model.

The difference of the lateral load versus displacement response of model A0 and A1 can be seen in Figure 4.9. During the anlysis of the cylces, it was seen that the element stresses of the A0 model almost attained its ultimate level with no energy dissipation, while having a lower load capacity than the A1 model. At the end of the cyclic loading, the crack patterns for the two models are shown in Figure 4.10 and 4.11.

After A1 model fulfilled its first reverse cycling, 6 mm diameter of wire mesh was installed and loaded again, leading to a new model that was named A1R. The peak load

capacity of the A1R model at the second-forward cycle was 281 kN. The A1 model achieved the maximum load of 221.5 kN at the first cycle loading due to assistance of the load capacity of the infill. Afterwards, the load capacity of the model began to fall down to 187.4 kN at around 14.4 mm in third forward-cycle loading, because of the crushed infill wall. Then, the RC frame of the A1 model maintained its loading capacity similar to the A0 model response. Nevertheless, the A1R model showed a ductile response during the analysis except for the initial cracks and longitudinal splitting of the infill wall that occurred at the top of the boundary of the RC frame. It can be understood from the simulation that the initial cracks did not develop until the peak lateral load capacity of the A1R model due to the presence of the installed wire mesh.

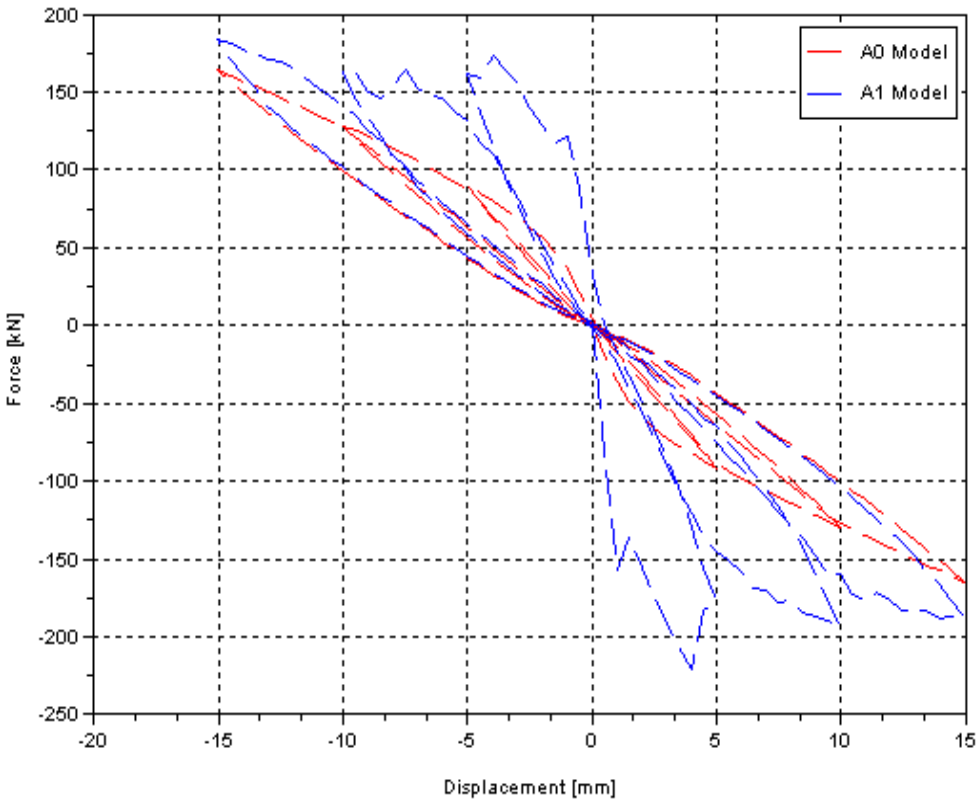

Figure 4.9. The lateral load versus displacement of A0-A1 models

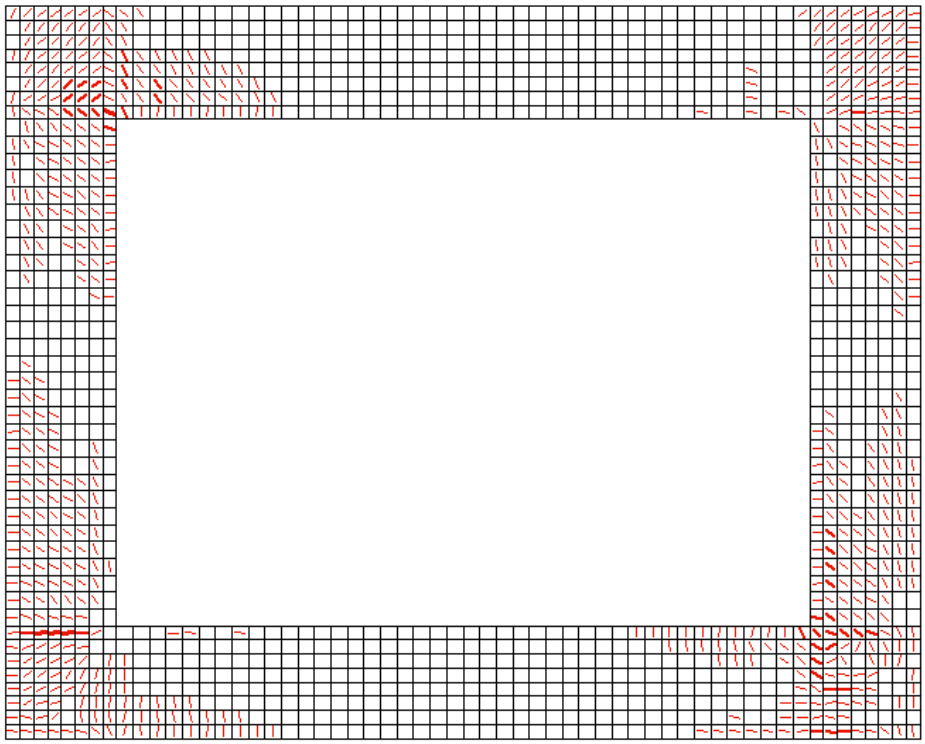

Figure 4.10. Crack patterns of A0 model

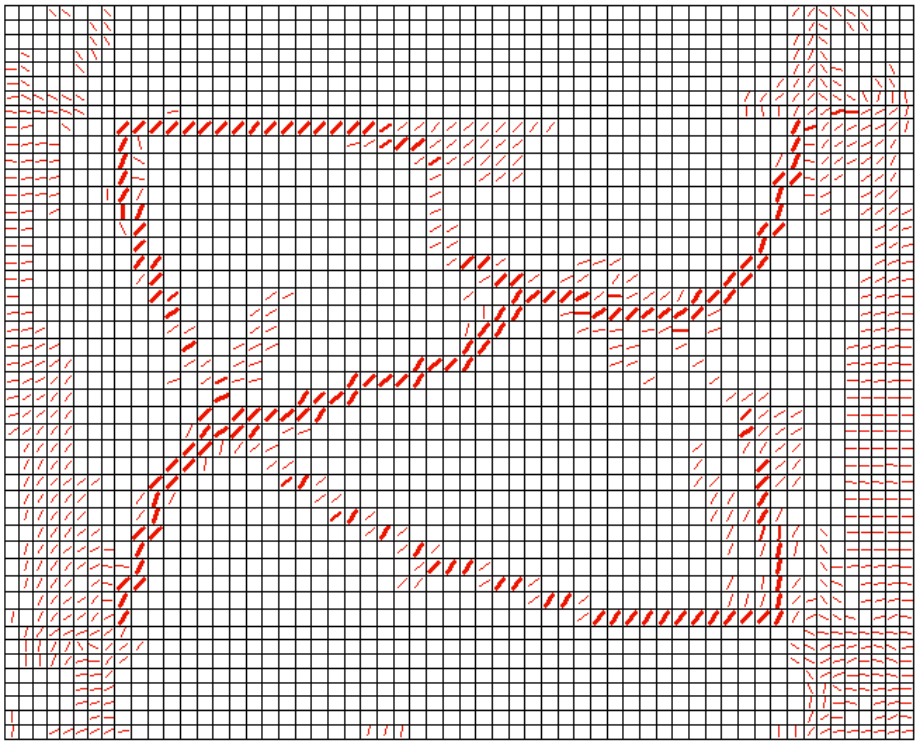

Figure 4.11. Crack patterns of A1 model

The wire mesh helped to distribute the tensile and compressive stresses, uniformly. For that reason, after the peak load had reached, initial cracks began to lengthen in their directions and crossed among the infill wall of the RC frame, no additional cracks occurred. This resulted in shear splitting of the infill that developed at the cracks and the edges of the frame.

The maximum average truss bar stresses were 428.3 MPa at the bottom part of the columns where they were yielded. And at the same points, average of 375.4 MPa of smeared transverse reinforcement stresses were seen at the interior side of column-beam joints. The maximum stresses of the concrete elements were 13.79 MPa at the bottom of the columns and top right beam-column joints. Peak lateral load capacity of the A1R model increased by 26% relative to the A1 peak lateral load capacity. Not only the lateral load capacity but also the energy dissipation increased, significantly. Figure 4.14. illustrates the comparisons of the lateral load and displacement of the A1 and A1R models. Figure 4.15 shows the crack patterns of A1R model.

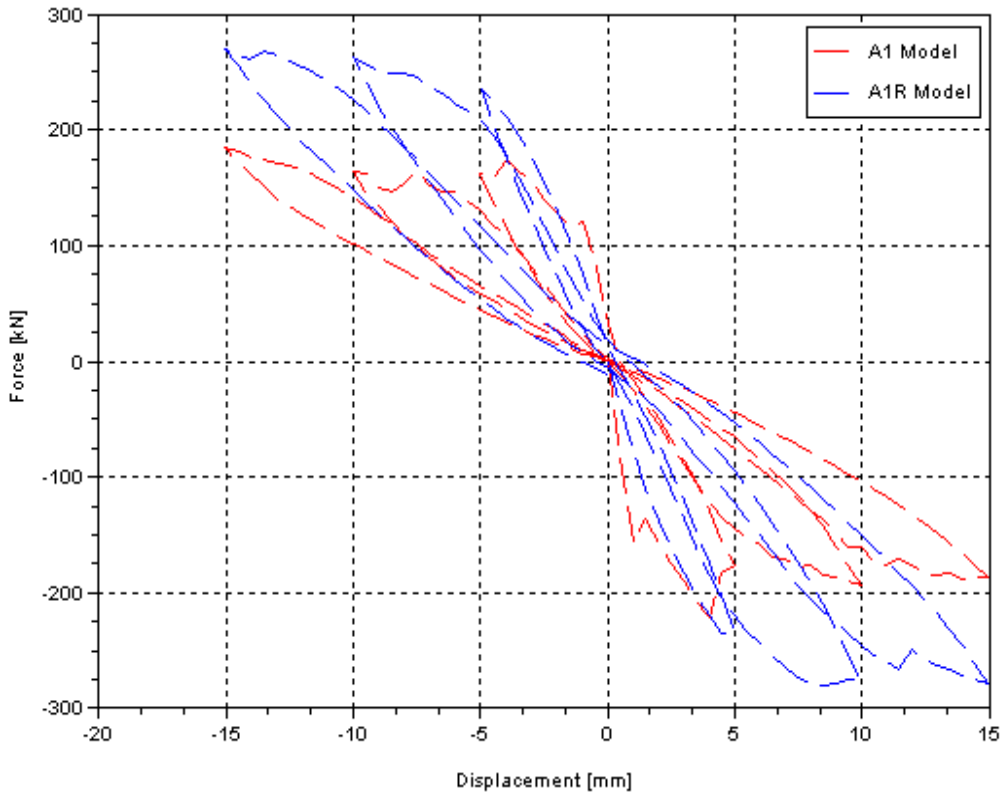

Figure 4.12. The lateral load versus displacement of A1-A1R models

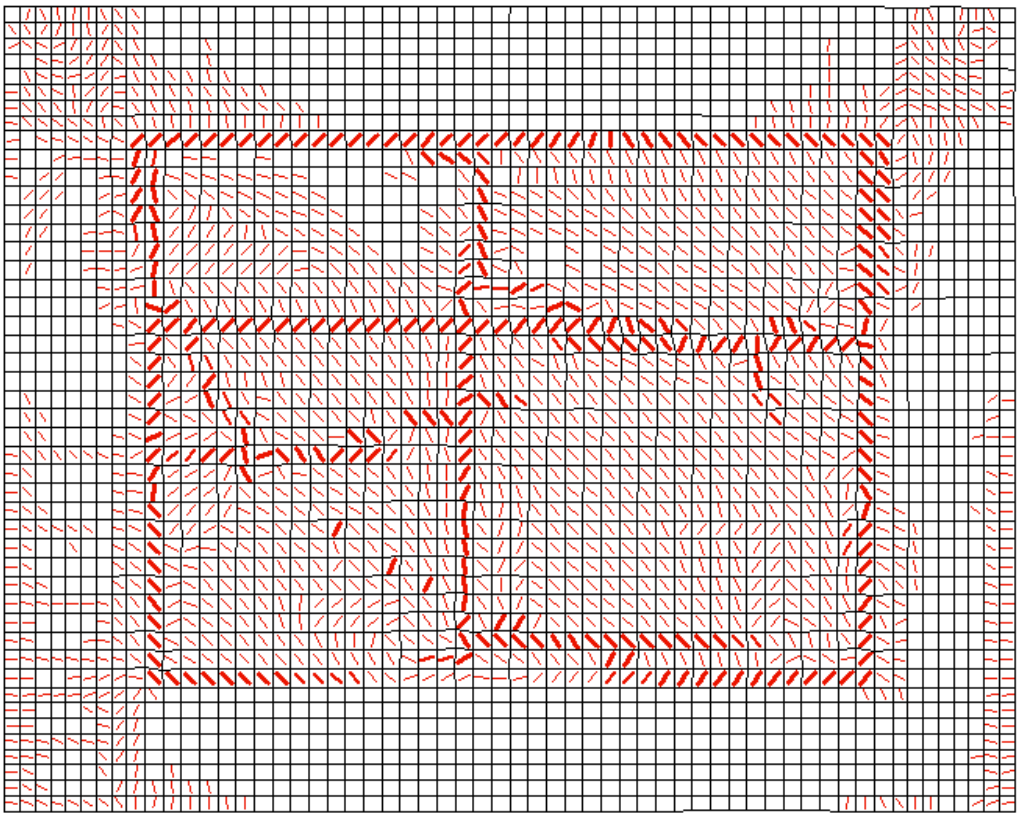

Figure 4.13. Crack patterns of A1R model

4.5.2. Analysis Results of Series B

In this series, the B1 and B2 models were installed with two different steel wire mesh sizes, 3 and 6 mm in diameter, respectively. The wire mesh was clamped to the RC frame. Similiar to the A1 model, the B1 model exhibited compression bars at the diagonals of the RC frame. And shear cracks occurred at this direction. Before cracking, the maximum load of 228.1 kN was reached at around 3 mm in the first forward cycle loading. The occurred cracks were transformed into longitudinal splitting cracks along the web of the infill. The wire mesh appeared to help in obtaining a more uniformly stress distribution in the infill wall, because no additional cracks were formed in other locations. The maximum average truss bar stresses were 478.2 MPa at the bottom part of the columns, beam-column connections and edges and the web of the

wire mesh, whereas local shear failures and yielding of reinforcement were seen. These events could result in bar dowel action in the reinforcement. 382.1 MPa of smeared transverse reinforcement stresses were visualized at the column-beam joints. The maximum stresses of the concrete elements were 12.36 MPa at the bottom part of the columns, as it was seen in the A1 model response. It can be understood that the reinforcement assisted the concrete. The B1 model developed its ductility during the end of the reverse cycle loading.

The maximum average truss bar stresses of the B2 model were 420 MPa (bars yielded) at the bottom of the columns and the edges of the frame. 391.3 MPa of smeared transverse reinforcement stresses were seen at the interior part of the top column-beam joints. The maximum stresses of the concrete elements were 13.75 MPa at the bottom part of the exterior side of the columns and top right of the beam-column joints. At the second forward cycle loading, before the boundary splitting at the opposite edges, a peak load of 326.2 kN was reached at 5.97 mm. The B1 model only reached a maximum peak load of 228.1 kN at 3 mm displacement. Distribution of stresses by wire mesh leaded to longitudinal shear splitting in the middle of infill due to high reinforcement tension stresses. And then longitudinal boundary splitting of the infill was seen. The maximum peak lateral load capacity of the B2 model was 42% larger than the capacity of the B1 model. The energy dissipation increased, as well. Figure 4.16. illustrates the comparison of the lateral load and displacement of the B1 and B2 models. In the A1R model, the first and second cycles fallen behind B2 model related with the lateral load capacity because of the presence of the initial cracks and initial stresses of A1R model. In the third cycle, A1R model reached similar capacity but the truss elements had more stresses than B2 model. Figure 4.15. shows the comparisons of the lateral load and displacement of the A1R and B2 models. Figure 4.16 and 4.17 show the crack patterns of B1 and B2 models.

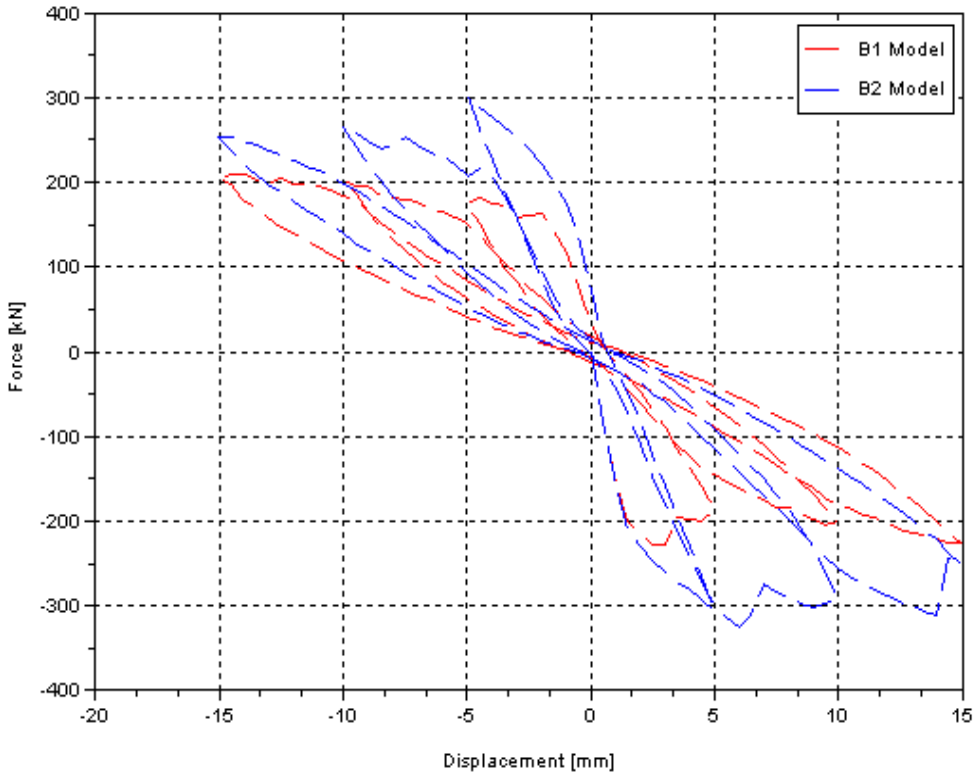

Figure 4.14. The lateral load versus displacement of B1-B2 models

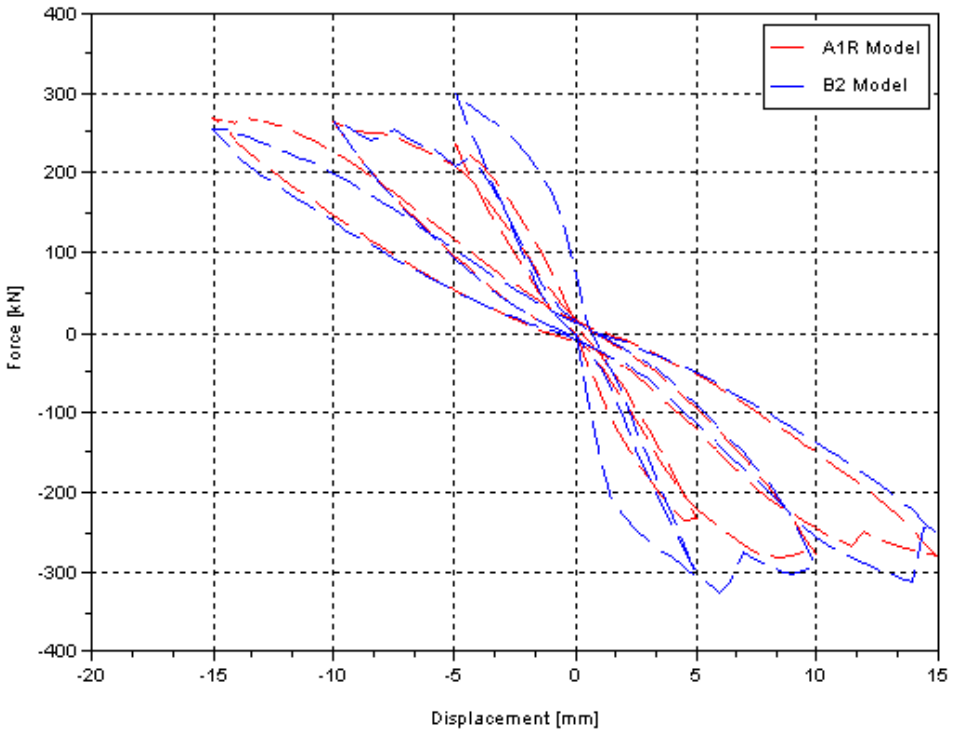

Figure 4.15. The lateral load versus displacement of B2-A1R models

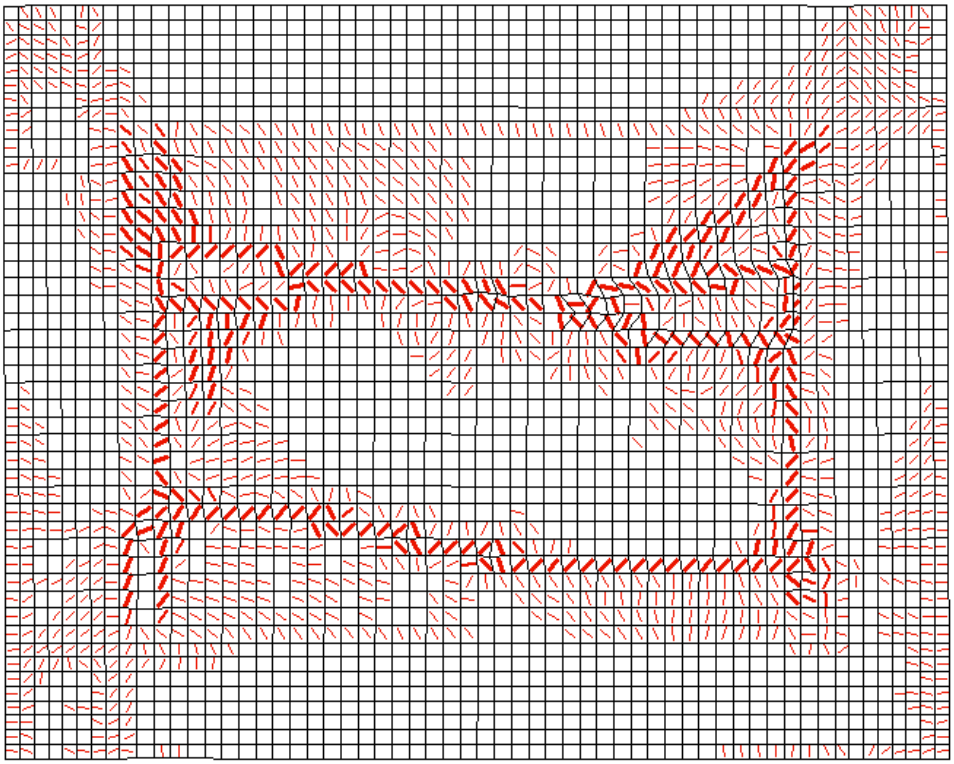

Figure 4.16. Crack patterns of B1 model

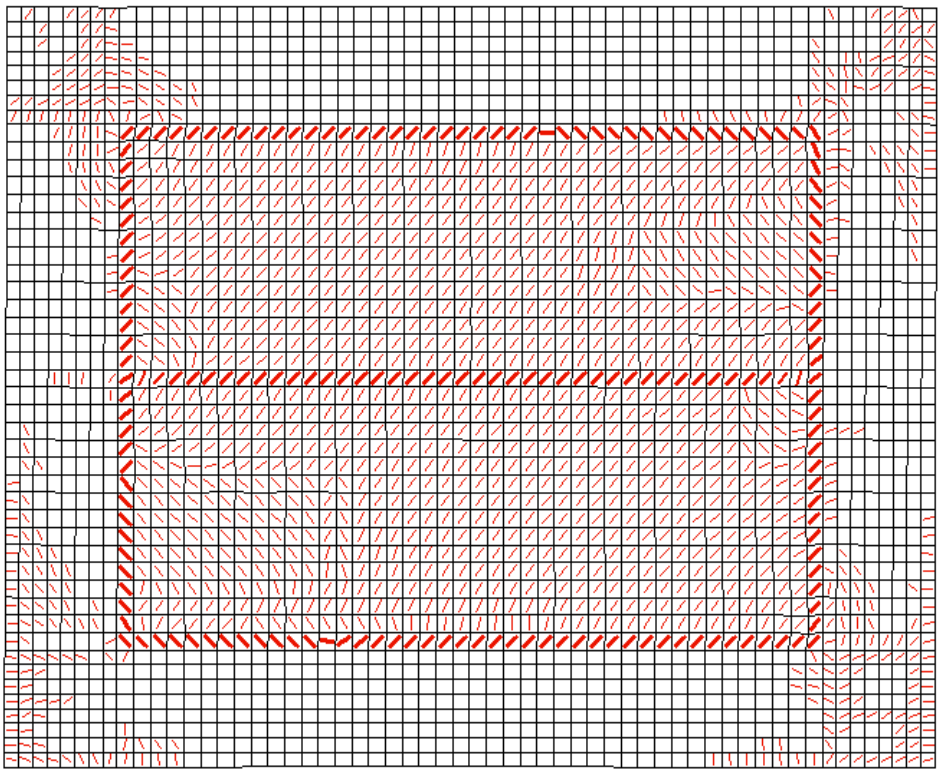

Figure 4.17. Crack patterns of B2 model

4.5.3. Analysis Results of Series C

The C series differed from the B series in terms of installation of the wire mesh that was not clamped to the RC frame. In the C1 model, the failure mode mechanism of the infill brikcs is similar to the B1 model. In the first forward cycle loading, before diagonal shear cracks occurred, a peak load of 223.1 kN was reached at around 2.49 mm top displacement. During the increasing repetitions of the loading, the diagonal shear cracks widened and the infill was longitudinal splitted at the middle of the infill wall. In addition to the longitudinal splitting, the boundary of the infill wall was splitted from the RC frame. As was expected, the infill wall contributed to the RC frame stiffness as the compression bar was established at the diagonals of the infill during the final stages of loading. The maximum average truss bar stresses of the C1 model were 379 MPa at the longitudinal bar of the columns. The smeared transverse reinforcement had maximum stress values of 410 MPa, which were seen at the interior and exterior part of the column-beam joints. The maximum stresses of the concrete elements were 12.49 MPa at the bottom part of the exterior side of the columns and top part of the interior beam-column joints

The response of the model C2 was similar to the model C1 response under hysteric loading. The maximum average truss bar stresses of C2 model were 393.4 MPa at the longitudinal bar of the columns and 414.1 MPa of smeared transverse reinforcement stresses were seen at the interior and exterior side of column-beam joints. The maximum stresses of the concrete elements were 12.55 MPa at the bottom part of the exterior side of the columns and top part of the interior beam-column joints. The wire mesh reinforcement did not contribute to stiffness of the frame in both models. The peak lateral load capacity of the models were a bit higher than in the A1 model. The boundary of the infill wall was splitted from the layer of RC frame completely.

The Figure 4.18 shows the simulation response of the lateral load vs. displacement of the C1 and C2 models. Figure 4.19 and 4.20 shows the crack patterns of C1 and C2 models.

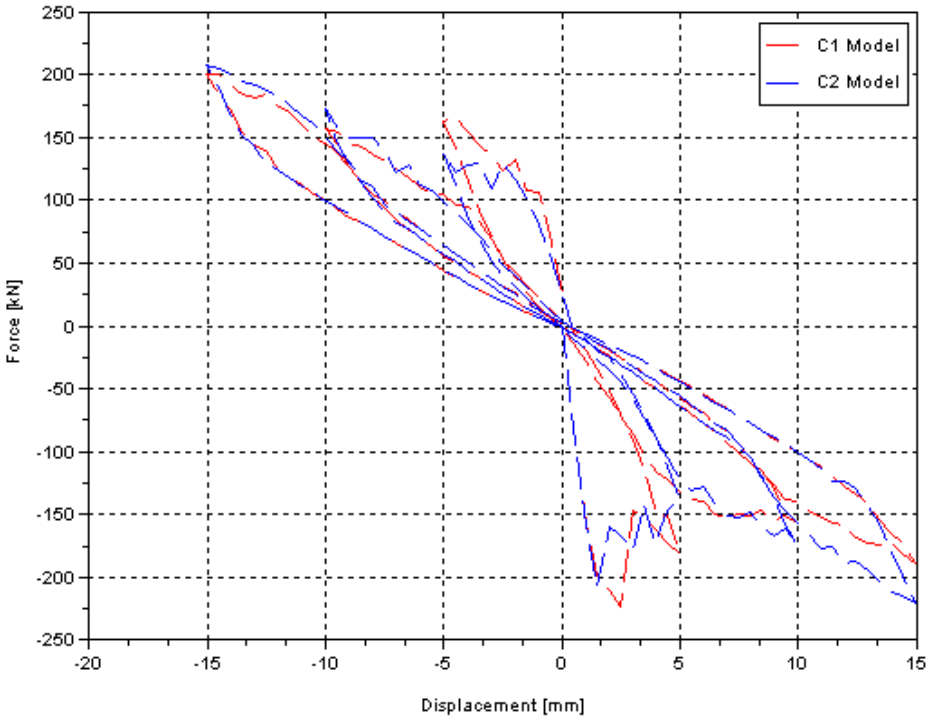

Figure 4.18. The lateral load versus displacement of C1-C2 models

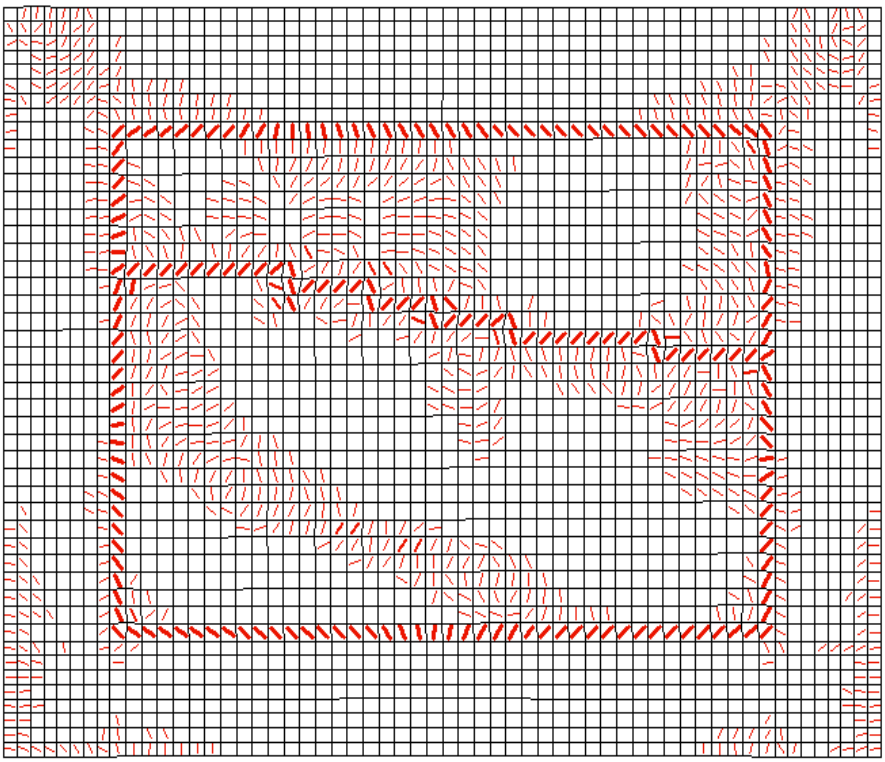

Figure 4.19. Crack patterns of C1 model

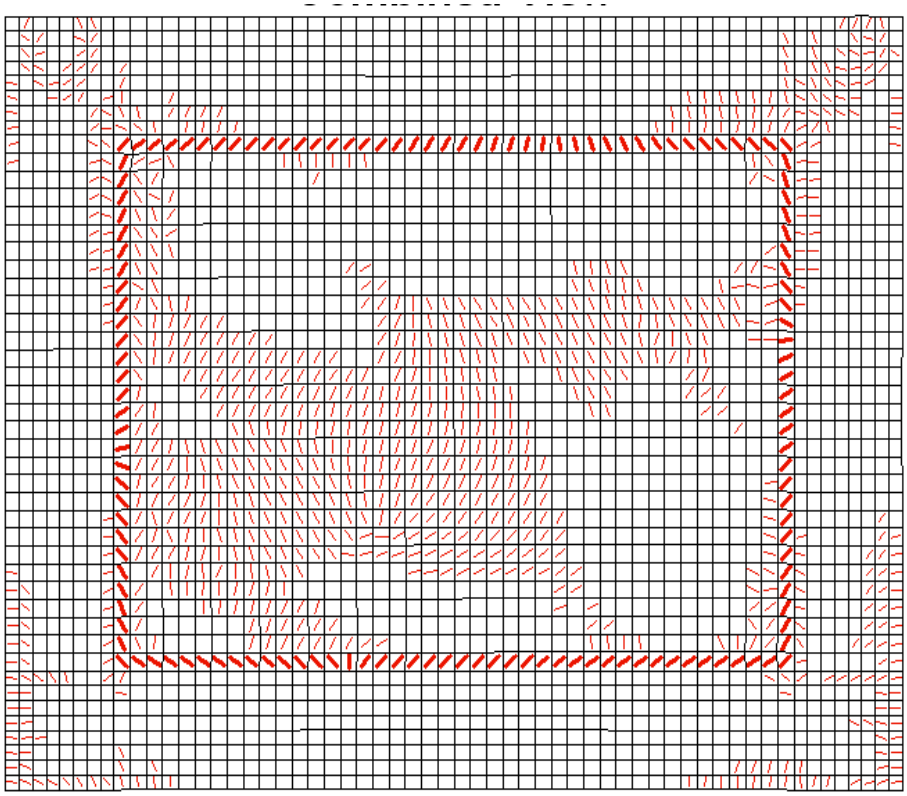

Figure 4.20. Crack patterns of C2 model

4.5.4. Discussion of the Results

Under the reverse cyclic loading, the forward cycle loading results were higher than the reverse cycle loading results. The analysis revealed higher forward loading resistance than reverse loading resistance because of the hysteretic response. Wire mesh installation (if clamped to the RC frame), effectively increased the load capacity of the infilled RC frame. It caused a uniformly stress distribution in the infill wall, and reduced the stress levels of the longitudinal and transverse reinforcement in the columns and beams. Local yielding of the reinforcement occurred at the location of shear splitting and this could cause the dowel action of the reinforcement.Before the shear splitting, compression bar was occurred at the infill and increased the lateral load capacity. If the compression bar widh lengthens the lateral loading capacity could be increased much more.

Wire mesh reinforcement added ductility to the infilled RC frame, and lengthened the load-displacement curve. Thus, a larger energy dissipation capacity was obtained. But, in order to obtain a benefit from the wire mesh, it has to be fastened to the outer RC frame. This can be done in a number of ways. One o them could be the usage of plates that are connected to the interior sides of the beams and columns, with the wire mesh joined to the plates.

CHAPTER 5

CONCLUSION

This study determined the advantage and disadvantages of strengthening an infill wall with wire mesh. Simulations were performed within a nonlinear finite element program, Vector2. The analysis results of the applied strengthening models ensures the improvement of energy dissipation, and increase in the lateral load capacity. The simulations of a number of infilled RC frames showed that the application of wire mesh on to the face of the brick wall, had beneficial effects. But the increase in load capacity and energy absorption only took place if the wire mesh was connected to the RC frame. In addtion, the wire mesh percentage has to be above a specific threshold.

Some difficulties were occurred before the beginning of the simulation. Testing procedure was limited due to inadequate testing machines and calibrated software. For this reason, uniaxial compressive strength of the infill blocks with the plaster layer could not be assessed. And also a prototype of RC frame could not be built and tested for the verification of the analytical models that are described in this thesis.

5.1. Proposed Future Work

Manufacturing RC frames and conduting an experimental work will be significant to compare the results of the computational studies. With these prototypes, different experimental retrofitting techniques would be tried. The retrofitting technique would focus on the connections of installation, especially for shear. Some analysis results indicated that shear splitting were seen at the boundary of the strengthening whereas the infill preserved its strength. If the connections are inadequate in strength, it is no need to be strengthened.

REFERENCES

Alcocer, S.M, Flores, L., Duran, R.1996. Recent Experimental Evidence On The Seismic Performance Of Rehabilitation Techniques In Mexico. *Advances in Earthquake Engineering for Urban Risk Reduction* 261-274.

Almusallam, T.H., Al-Salloum, Y.A., 2006. Behavior of FRP Strengthened Infill Walls under In-Plane Seismic Loading. *Journal of Composites for Construction* 11:3(308).

Altın, S., Anıl, Ö., Kara, M.E., Kaya, M., 2007. An experimental study on strengthening of masonry infilled RC frames using diagonal CFRP strips.*Composites: Part B* 39:680-693.

Altın, S., Anıl, Ö., Kara, M.E., 2007. Strengthening of RC nonductile frames with RC infills: An Experimental Study. *Cement & Concrete Composites* 10:1016/j.

Anıl, Ö., Altın, S., 2006. An experimental study on reinforced concrete partially infilled frames. *Engineering Structures* 29:449-460.

Bodycote Testing Mechanical Testing of Bricks. http:///mt.bodycote.com/?OB=112&POB=84&ID=207 (accesseed May 09, 2008).

Binici, B., Özcebe, G., Özçelik, R., 2007. Analysis and design of FRP composites for seismic retrofit of infill walls in reinforced concrete frames.*Composites: Part B* 10:1016/j.

Canbay, E., U., Ersoy, Özcebe, G., 2003. Contribution of Reinforced Concrete Infills to Seismic Behavior of Structural Systems. *ACI Structural Journal* 100-S66

Erdem, İ., Akyüz, U., Ersoy, U., Özcebe, G., 2006. An experimental study on two different strengthening techniques for RC frames. *Engineering Structures* 28:1843-1851.

Ersoy, U., 2001. *Betonarme*. İstanbul: Evrim Yayınevi

Garevski M., Hristovski, V., Stojmanovska, M., 2006. Shaking Table Tests Of Scaled RC Frame Models For Investigation Of Validity And Applicability Of Different Retrofitting Techniques. *Springer* 441- 453.

Palermo, D. and Vecchio, F.J., 2006. Simulation of Cyclically Loaded Concrete Structures Based on the Finite-Element Method. *Journal of Structural Engineering* 133:5(728).

Saatçioğlu, M., 2006. Seismic Risk Mitigation Through Retrofitting Nonductile Concrete Frame Systems. *Advances in Earthquake Engineering for Urban Risk Reduction* 179-194.

Shing, P.B., Mehrabi, A.B., 2002. Behaviour and analysis of masonry-infilled frames. *Program Structural Engineering Material* 4:320-331.

US Army Corps of Engineers, 2008. Standard Test Methods for Compressive Strength of MasonryPrisms. http://www.wes.army.mil/SL/MTC/handbook/CRD_C643.pdf (accessed May 12, 2008).

Tankut, T., Ersoy, U., Özcebe, G., Baran, M., Okuyucu, D., 2006. In Service Seismic Strengthening Of RC Framed Buildings. *Advances in Earthquake Engineering for Urban Risk Reduction* 47-62.

TS 4563, *Turkish Code of Horizontal Coring Bricks*, 1986.

TS 500, *Turkish Design Code* 2006.

Turkish Earthquake Code 2006.

Türk, M., Ersoy, U., Özcebe, G., 2003. Seismic Rehabilitation Of RC Frames With RC Infill Walls. *Fifth National Conference on Earthquake Engineering*, İstanbul, Turkey AT-045.

Vecchio, F.J. and Collins, M.P., 1986. The Modified Compression Field Theory for Reinforced Concrete Elements Subjected to Shear. *ACI Journal*. 83-22.

Vecciho, F.J., 1989. Nonlinear Finite Element Analysis of Reinforced Concrete Membranes. *ACI Structural Journal* 86 S4.

Vecchio, F.J., Lai, D., Shim, W., Ng, J., 2001. Disturbed Stress Field Model for Reinforced Concrete: Validation. *Journal of Structural Engineering* 127 4:350-358.

Vecciho, F.J. and Shim, W., 2004. Experimental and Anaytical Reexamination of Classic Concrete Beam Tests. *Journal of Structural Engineering* 130 3: 460-469.

Wong, P. S., and Vecchio, F.J., 2002. VecTor2 and Formworks User's Manual. *University of Toronto, Department of Civil Engineering Publications.*

APPENDIX A

DETERMINING MOMENT-DISPLACEMENT OF RC FRAME

Table A.1. Scilab Code (Modified Kent-Park Model)

```
***

//determining neutral axis depth c

fck=14;                          //characteristic cylinder strenngth (MPa)
fc=fck;                          //peak compressive strength (MPa)
h=500;                           //height of the cross section (mm)
dc=62.5;                         //cover thickness of the concrete (mm)
bw=250;                          //width of the cross section (mm)
d=h-dc;                          //mm

Ec=126800+460*fc;                //young modulus of the concrete (MPa)
Es=2*10E^5;                      //young modulus of the steel (MPa)
epsilon_sy=0.002;                //yield strain of the steel bar
epsilon_cu=-0.004;               //ultimate  strain of the concrete
epsilon_c0=-0.002;               //yield  strain of the concrete
inc=-0.0001;                     //size of increment

epsilon_c=inc:inc:epsilon_cu;    //must be negative sign while all in compression
As1=615.7;                       //tension longitudinal reinforcement (mm^2)
As2=615.7;                       //compression longitudinal reinforcement (mm^2)
spc=400;                         //stirup spacing (mm)
Ass=54.8;                        //stirup diameter (mm^2)
b=bw-dc;                         //minimum length of the inner concrete zone (mm)
a=h-dc;                          //minimum length of the inner concrete zone (mm)
ro=(Ass*2*(a+b))/(spc*a*b);      //ratio of the volume of the stirups to concrete
```

(cont. on next page)

Table A.1.(cont.) Scilab Code (Modified Kent-Park Model)

```
for j=1:length(epsilon_c);

//intervals of the function c(1)and c(2)

c(1,j)=h/100;                 //for bisection method ftotal(1)should be with negative sign
c(2,j)=h;                     //for bisection method ftotal(2) should be with positive sign
c(3,j)=0.5*(c(1)+c(2));       //first midstep of the function in bisection method

end

step=100;                     //max number of iterations

range_i=1:3;
for s=1:step
 if s>2 then

//ıf s=1 Ftotal(1,2,3)
//ıf s>1 old Ftotal(1),old Ftotal(2) new Ftotal(3)

range_i=3;
end
for i=range_i;
      for j=1:length(epsilon_c);
      epsilon_s1(i,j)=epsilon_c(j)*(d-c(i,j))/c(i,j)  ;
      epsilon_s2(i,j)=epsilon_c(j)*(dc-c(i,j))/c(i,j) ;

// tension is positive, compression is negative

      if abs(epsilon_s1(i,j))>epsilon_sy then
      epsilon_s1(i,j)=epsilon_sy *(epsilon_s1(i,j)/abs(epsilon_s1(i,j)));
      end
      if abs(epsilon_s2(i,j))>epsilon_sy then
       epsilon_s2(i,j)=epsilon_sy *(epsilon_s2(i,j)/abs(epsilon_s2(i,j)));
       end
      sigma_s1(i,j)=Es*epsilon_s1(i,j);
      Fs1(i,j)=As1*sigma_s1(i,j);
      sigma_s2(i,j)=Es*epsilon_s2(i,j);
      Fs2(i,j)=As2*sigma_s2(i,j);
```

(cont. on next page)

Table A.1.(cont.) Scilab Code (Modified Kent-Park Model)

```
****

//obtaining modified Kent-Park curve

      if epsilon_c(j)>=epsilon_c0 then
      sigma(j)=fc*(2*epsilon_c(j)/epsilon_c0-(epsilon_c(j)/epsilon_c0)^2);
      else
      epsilon50u=(.3+0.0285*fc)/(14.2*fc-100);
      epsilon50h=(3/4)*ro*sqrt(b/s);
      Z=0.5/(epsilon50u+epsilon50h-abs(epsilon_c0));
      sigma(j)=fc*(1-Z*(abs(epsilon_c(j))-abs(epsilon_c0)));
      end

  if j==1 then
     A(j)=0.5*(sigma(j));
     Ac(j)=A(j);
     else
     A(j)=0.5*(sigma(j)+sigma(j-1));
     Ac(j)=Ac(j-1)+A(j);
     end
     Fc(i,j)=Ac(j)*bw*c(i,j)/j;
     Ftotal(i,j)=Fc(i,j)+Fs2(i,j)+Fs1(i,j);
    end
end


***

//bisection method

//find points a and b such that a<b and f(a)*f(b)<0
//take interval[a b] and find its midpoint x1
//ıf(x1)=0 then x1 is the exact root,elseif f(x1)*f(b)<0 then a=x1
//elseif f(a)*f(x1)<0 then let b=x1
//repeat steps until f(xi)=0 or |f(xi)|<=degree of accuracy


for j=1:length(epsilon_c)
   if Ftotal(1,j)*Ftotal(2,j)<0 then
      if Ftotal(3,j)*Ftotal(2,j)<0
       c(1,j)=c(3,j);
       Ftotal(1,j)=Ftotal(3,j);
       else //Ftotal(1)*Ftotal(3)<0 then
       c(2,j)=c(3,j);
       Ftotal(2,j)=Ftotal(3,j);
       end
```

(cont. on next page)

Table A.1.(cont.) Scilab Code (Modified Kent-Park Model)

```
end
end
  for j=1:length(epsilon_c);
      c(3,j)=0.5*(c(1,j)+c(2,j));
  end
   if abs(Ftotal(3,:))<0.0001 then
      disp(c,Ftotal,s)
      break
   end

   if s==step then
      break
      disp("step size exceeded")
   end


****

//moment-curvature

     for j=1:length(epsilon_c);
      K(i,j)=epsilon_c(j)/c(i,j);
      Ms(i,j)=(Fs1(i,j)-Fs2(i,j))*(0.5*h-dc);
      Mc(i,j)=-Fc(i,j)*(0.5*h-c(i,j)/2);
      M(i,j)=Mc(i,j)+Ms(i,j);
      end

end

//moment-displacement

yp=9;                                          //yield point
colL=1125;                                     //half length f the column (mm)
K=K(3,:);
M=M(3,:);
Myield=abs(M(yp));
Kyield=abs(K(yp));
[a,b]=size(K);
```

(cont. on next page)

Table A.1.(cont.) Scilab Code (Modified Kent-Park Model)

```
helper1=0;helper2=0;
for i=1:b
  if abs(K(i))<Kyield  then //elastic
    delta(i)=(1/3)*abs(K(i))*colL^2;helper1=helper1+1;
  else //inelastic
    x=colL-colL*Myield/abs(M(i));helper2=helper2+1;


delta(i)=(Kyield*(colL-x)^2)/3 + Kyield*x*(colL-x/2) + (abs(K(i))*x/2)*(col
+(2/3)*x);
end
end
subplot(121);plot(-K,-M); xtitle('','Curvature (rad/mm)','Moment (N mm)');plot(-K,-
M,'.');
subplot(122);plot(delta,-M); xtitle('','Relative Displacement(mm)','Moment (N
mm)');plot(delta,-M,'.');

plot((dx,Md,'r--',delta,-M,'b--'); xtitle('','Displacement [mm]',' Moment [Nmm]');
legend('Analytical Model','Modified Kent-Park Model');xgrid(1)
```